

RankFeat&RankWeight: Rank-1 Feature/Weight Removal for Out-of-distribution Detection

Yue Song, *Member, IEEE*, Wei Wang, *Member, IEEE*, Nicu Sebe, *Senior Member, IEEE*

Abstract—The task of out-of-distribution (OOD) detection is crucial for deploying machine learning models in real-world settings. In this paper, we observe that the singular value distributions of the in-distribution (ID) and OOD features are quite different: the OOD feature matrix tends to have a larger dominant singular value than the ID feature, and the class predictions of OOD samples are largely determined by it. This observation motivates us to propose RankFeat, a simple yet effective *post hoc* approach for OOD detection by removing the rank-1 matrix composed of the largest singular value and the associated singular vectors from the high-level feature. RankFeat achieves *state-of-the-art* performance and reduces the average false positive rate (FPR95) by 17.90% compared with the previous best method. The success of RankFeat motivates us to investigate whether a similar phenomenon would exist in the parameter matrices of neural networks. We thus propose RankWeight which removes the rank-1 weight from the parameter matrices of a single deep layer. Our RankWeight is also *post hoc* and only requires computing the rank-1 matrix once. As a standalone approach, RankWeight has very competitive performance against other methods across various backbones. Moreover, RankWeight enjoys flexible compatibility with a wide range of OOD detection methods. The combination of RankWeight and RankFeat refreshes the new *state-of-the-art* performance, achieving the FPR95 as low as 16.13% on the ImageNet-1k benchmark. Extensive ablation studies and comprehensive theoretical analyses are presented to support the empirical results. Code is publicly available via <https://github.com/KingJamesSong/RankFeat>.

Index Terms—Distribution Shift, Out-of-distribution Detection

1 INTRODUCTION

In the real-world applications of deep learning, understanding whether a test sample belongs to the same distribution of training data is critical to the safe deployment of machine learning models. The main challenge stems from the fact that current deep learning models can easily give over-confident predictions for out-of-distribution (OOD) data [1]. Recently a rich line of literature has emerged to address the challenge of OOD detection [2], [3], [4], [5], [6], [7], [8], [9], [10], [11], [12], [13], [14], [15], [16], [17], [18], [19], [20], [21], [22], [23].

Previous OOD detection approaches either rely on the feature distance [24], activation abnormality [6], or gradient norm [3]. In this paper, we tackle the problem of OOD detection from another perspective: by analyzing the spectrum of the high-level feature matrices (e.g., the output of Block 3 or Block 4 of a typical ResNet [25] model), we observe that the feature matrices have quite different singular value distributions for the in-distribution (ID) and OOD data (see Fig. 1(a)): *the OOD feature tends to have a much larger dominant singular value than the ID feature, whereas the magnitudes of the remaining singular values are very similar*. This peculiar behavior motivates us to remove the rank-1 matrix composed of the dominant singular value and singular vectors from the feature. As displayed in Fig. 1(b), removing the rank-1 feature drastically perturbs the class prediction of OOD samples; a majority of predictions have been changed. On the contrary,

most ID samples have consistent classification results before and after removing the subspace. *This phenomenon indicates that the over-confident prediction of OOD samples might be largely determined by the dominant singular value and the corresponding singular vectors.*

Based on this observation, we **assume** that the first singular value of the OOD feature tends to be much larger than that of the ID feature. The intuition behind this is that the OOD feature corresponds to a larger Principal Component Analysis (PCA) explained variance ratio (being less informative), and the well-trained network weights might cause and amplify the difference (see Sec. D of the supplementary for the detailed illustration). Hence, we conjecture that leveraging this gap might help to better distinguish ID and OOD samples. To this end, we propose RankFeat, a simple but effective *post hoc* approach for OOD detection. RankFeat perturbs the high-level feature by removing its rank-1 matrix composed of the dominant singular value and vectors. Then the logits derived from the perturbed features are used to compute the OOD score function. By removing the rank-1 feature, the over-confidence of OOD samples is mitigated, and consequently the ID and OOD data can be better distinguished (see Fig. 3). Our RankFeat establishes the *state-of-the-art* performance on the large-scale ImageNet benchmark and a suite of widely used OOD datasets across different network depths and architectures. In particular, RankFeat outperforms the previous best method by **17.90%** in the average false positive rate (FPR95) and by **5.44%** in the area under curve (AUROC). Extensive ablation studies are performed to reveal important insights of RankFeat, and comprehensive theoretical analyses are conducted to explain the working mechanism.

The success of RankFeat implies that a similar abnor-

• Yue Song and Nicu Sebe are with Department of Information Engineering and Computer Science, University of Trento, Trento 38123, Italy. Wei Wang is with Beijing Jiaotong University, Beijing, China. Wei Wang is the corresponding author.
E-mail: {yue.song, nicu.sebe}@unitn.it, wei.wang@bjtu.edu.cn

Manuscript received April 19, 2005; revised August 26, 2015.

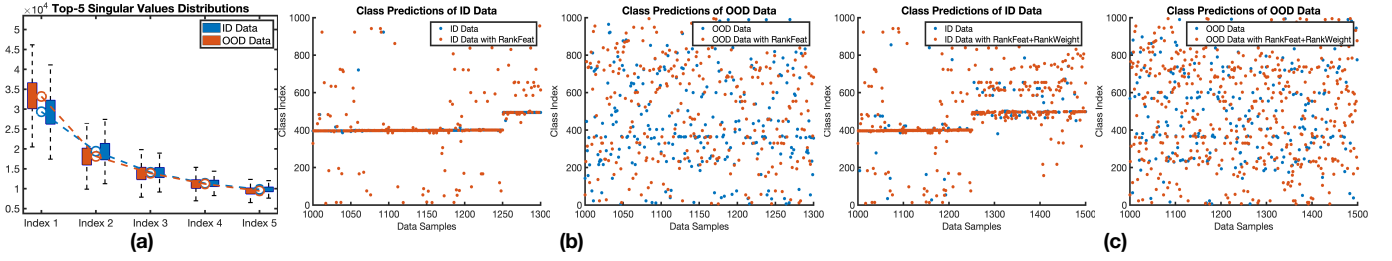


Fig. 1: (a) The distribution of top-5 singular values for the ID and OOD features on ImageNet-1k and SUN. The OOD feature matrix tends to have a significantly larger dominant singular value. (b) After removing the rank-1 matrix composed by the dominant singular value and singular vectors, the class predictions of OOD data are severely perturbed, while those of ID data are moderately influenced. This observation indicates that the decisions of OOD data heavily depend on the dominant singular value and the corresponding singular vectors of the feature matrix. In light of this finding, we get motivated to propose RankFeat for OOD detection by removing the rank-1 matrix from the high-level feature. (c) After pruning the parameters of a single deep layer by removing the rank-1 matrix similarly, the class predictions of ID and OOD data exhibit distinct behaviors: most ID samples remain consistent class predictions, while OOD data is largely perturbed. This implies that the rank-1 parameter matrix of deep layers also plays a crucial role in making decisions about data samples. We thus propose RankWeight for *post hoc* OOD detection by removing the rank-1 matrix from the deep parameter matrix of only one layer. The observations also hold for other OOD datasets.

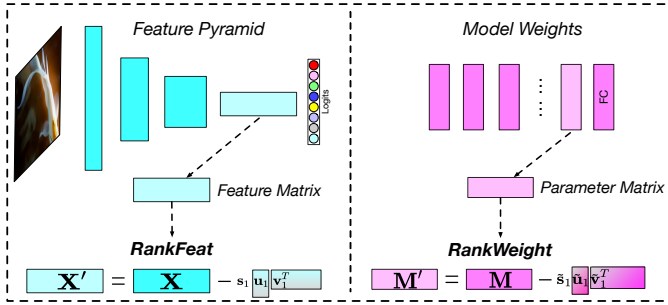


Fig. 2: Visual illustration of our RankFeat and RankWeight: RankFeat removes the rank-1 **feature matrix** from the deep layers, while RankWeight perturbs the **weight matrix** of deep layers by removing the rank-1 subspace similarly.

ality of the rank-1 matrix might also exist in other aspects of deep learning models such as the parameter matrices of deep network layers. To investigate this research question, we also measure the impact of the rank-1 parameter matrix on the model decisions. As can be seen from Fig. 1(c), the class predictions are also largely dependent on the rank-1 matrix of deep parameters; pruning the parameter matrix would heavily perturb the model decisions. This observation implies that the over-confidence of OOD samples might be closely related to the rank-1 parameter matrix. In light of this finding, we propose RankWeight, another simple yet effective *post hoc* OOD detection approach which removes the rank-1 weight matrix from the last deep parameter matrix before the fully-connected layer. Fig. 2 illustrates the working mechanisms of our RankFeat and RankWeight. Compared with RankFeat, RankWeight is more computationally efficient as it only requires (approximate) matrix decomposition once for only one layer of the model. When RankWeight is used standalone, it establishes competitive performance against previous baselines. Moreover, our RankWeight can be integrated with a wide range of OOD detection methods and boost their performance, including GradNorm [3], ReAct [6], ASH [18], VRA [26], and our RankFeat. For

example, combining RankWeight and RankFeat attains an FPR95 of 16.13% and an AUROC of 96.20%, and integrating RankWeight into ASH [18] attains an FPR95 of 15.46% and an AUROC of 97.13%, both of which achieve new *state-of-the-art* performance across datasets on ImageNet-1k benchmark. We conduct some ablation studies to understand the impact of pruning different layers using RankWeight. Also, some theoretical analyses are performed to show that performing RankWeight can tighten the score upper bound.

The **key results and main contributions** are threefold:

- We propose RankFeat and RankWeight, two simple yet effective *post hoc* approaches for OOD detection by removing the rank-1 matrix from the high-level feature and deep parameter matrices, respectively. RankFeat achieves the *state-of-the-art* performance across benchmarks and models, reducing the average FPR95 by 17.90% and improving the average AUROC by 5.44% compared to the previous best method. Combining RankFeat and RankWeight further establishes *state-of-the-art* performance on the ImageNet-1k benchmark, achieving a low FPR95 of 16.13% and a high AUROC of 96.20%.
- We perform extensive ablation studies to illustrate the impact of (1) removing or keeping the rank-1 feature, (2) removing the rank- n feature ($n > 1$), (3) applying our RankFeat at various network depths, (4) the number of iterations to iteratively derive the approximate rank-1 matrix for acceleration but without performance degradation, (5) different fusion strategies to combine multi-scale features for further performance improvements, and (6) pruning different number of layers using RankWeight.
- Comprehensive theoretical analyses are conducted to explain the working mechanism and to underpin the superior empirical results. We show that (1) removing the rank-1 feature reduces the upper bound of OOD scores more, (2) removing the rank-1 matrix makes the statistics of OOD feature closer to random matrices, (3) both RankFeat and ReAct [6] work by optimizing the upper bound containing the largest singular value. ReAct [6] indirectly and manually clips the underlying term, while

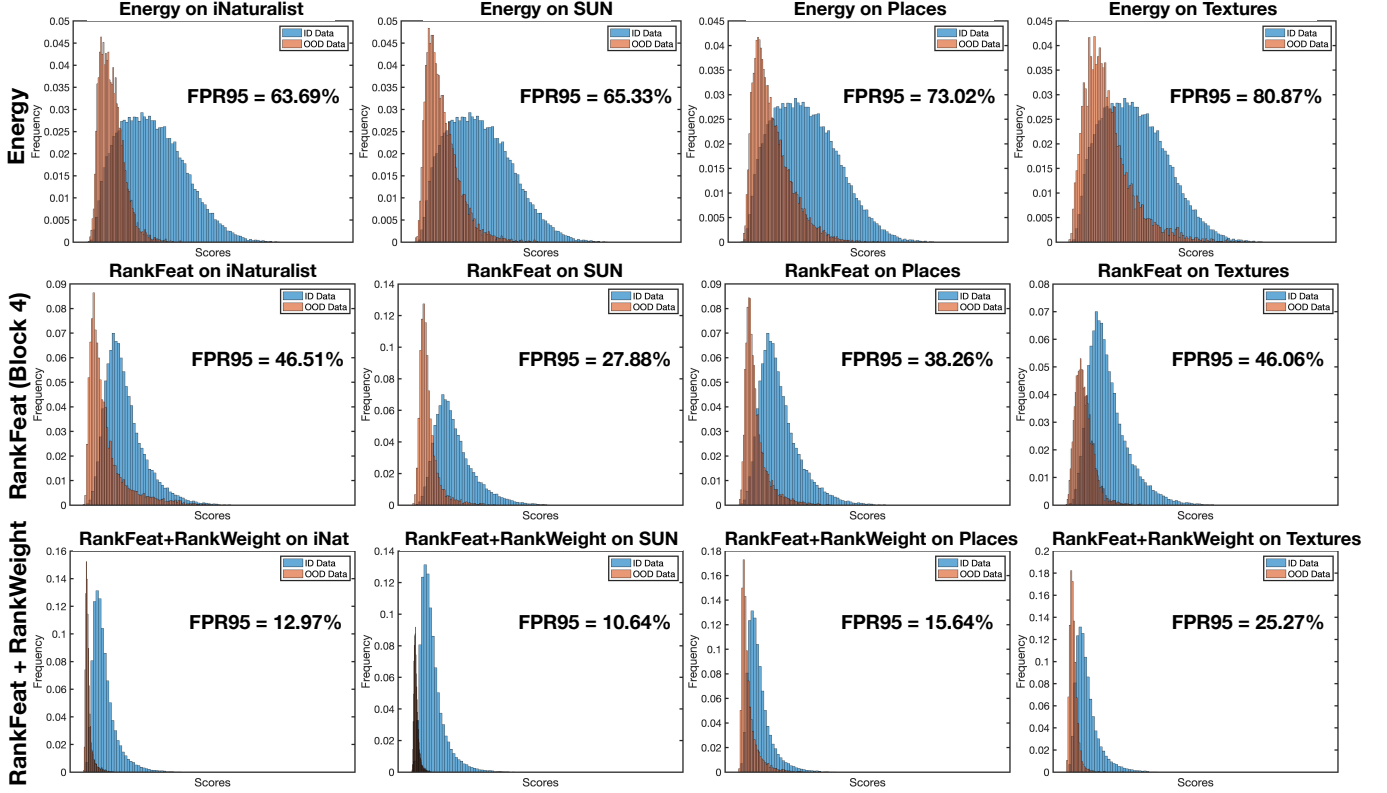


Fig. 3: The score distributions of Energy [27] (top row), our RankFeat (middle row), and our proposed RankFeat+RankWeight (bottom row) on four OOD datasets. Our method can better separate the ID and OOD data.

RankFeat directly subtracts it, and (4) our RankWeight can effectively tighten the score upper bound.

This paper is an extension of the previous conference paper [28]. In [28], we observe the abnormality of the rank-1 feature and propose RankFeat for OOD detection by removing the rank-1 matrix from the high-level feature maps. The journal extension validates that similar behavior can be also observed in the parameters of deep network layers, and further proposes RankWeight which performs OOD detection by pruning the rank-1 weight from the deep parameter matrices. Our RankWeight can be combined with many OOD detection methods, and particularly jointly applying RankFeat and RankWeight establishes the new *state-of-the-art* on the large-scale OOD detection benchmark. We also conduct some theoretical analysis and ablation studies to improve the understanding of RankWeight.

The rest of the paper is organized as follows: Sec. 2 describes the related work in distribution shifts and OOD detection. Sec. 3 introduces our proposed RankFeat and RankWeight which remove the rank-1 matrix from the deep feature maps and parameter matrices respectively, and Sec. 4 presents the theoretical analyses that underpin our methods. Sec. 5 provides experimental results and some in-depth analysis. Finally, Sec. 6 summarizes the conclusions.

2 RELATED WORK

2.1 Distribution Shifts

Distribution shifts have been a long-standing problem in the machine learning research community [29], [30], [31],

[32]. The problem of distribution shifts can be generally categorized as shifts in the input space and shifts in the label space. Shifts only in the input space are often deemed as *covariate shifts* [33], [34]. In this setting, the inputs are corrupted by perturbations or shifted by domains, but the label space stays the same [35], [36]. The aim is mainly to improve the robustness and generalization of a model [37]. For OOD detection, the labels are disjoint and the main concern is to determine whether a test sample should be predicted by the pre-trained model [35], [38].

Some related sub-fields also tackle the problem of distribution shifts in the label space, such as novel class discovery [39], [40], open-set recognition [41], [42], and novelty detection [43], [44]. These sub-fields target specific distribution shifts (*e.g.*, semantic novelty), while OOD encompasses all forms of shifts.

2.2 OOD Detection with Discriminative Models

The early work on discriminative OOD detection dates back to the classification model with rejection option [45], [46]. The OOD detection methods can be generally divided into training-need methods and *post hoc* approaches. Training-needed methods usually need auxiliary OOD data to regularize the model for lower confidence or higher energy [47], [48], [49], [50], [51], [52], [53], [54], [55], [56], [57]. Compared with training-needed approaches, *post hoc* methods do not require any extra training processes and could be directly applied to any pre-trained models. For the wide body of research on OOD detection, please refer to [58] for the comprehensive survey. Here we highlight some representative *post hoc* methods.

Nguyen *et al.* [1] first observed the phenomenon that neural networks easily give over-confident predictions for OOD samples. The following research attempted to improve the OOD uncertainty estimation by proposing ODIN score [38], OpenMax score [59], Mahalanobis distance [24], and Energy score [27]. Huang *et al.* [60] pointed out that the traditional CIFAR benchmark does not extrapolate to real-world settings and proposed a large-scale ImageNet benchmark. More recently, Sun *et al.* [6] and Huang *et al.* [3] proposed to tackle the challenge of OOD detection from the lens of activation abnormality and gradient norm, respectively. Following [6], recent works emerge to find the optimal activation shaping methods from various perspectives [18], [19], [26]. In contrast, based on the empirical observation about the impact of the dominant singular pairs on model decisions, we propose RankFeat and RankWeight, two simple yet effective *post hoc* solutions by removing the rank-1 subspace from the high-level features and deep parameter matrices, respectively. The technique of learning matrices has also been widely explored in various tasks of deep learning [61], [62], [63].

2.3 OOD Detection with Generative Models

Different from discriminative models, generative models detect the OOD samples by estimating the probability density function [4], [64], [65], [66], [67], [68], [69], [70]. A sample with a low likelihood is deemed as OOD data. Recently, a multitude of methods have utilized generative models for OOD detection [71], [72], [73], [74], [75], [76], [77]. Recent approaches focus on leveraging the power of generative models for synthesizing virtual outliers to regularize the decision boundary of ID and OOD samples [14], [78], [79]. However, as pointed out in [80], generative models could assign a high likelihood to OOD data. Furthermore, generative models can be prohibitively harder to train and optimize than their discriminative counterparts, and the performance is often inferior.

3 RANKFEAT&RANKWEIGHT: RANK-1 FEATURE/WEIGHT REMOVAL FOR OOD DETECTION

In this section, we introduce the background of OOD detection task and our proposed RankFeat and RankWeight that perform the OOD detection by removing the rank-1 matrix from the high-level feature and the deep parameter matrix, respectively.

3.1 Preliminary: OOD Detection

The OOD detection is often formulated as a binary classification problem with the goal to distinguish between ID and OOD data. Let f denote a model trained on samples from the ID data \mathcal{D}_{in} . For the unseen OOD data \mathcal{D}_{out} at test time, OOD detection aims to define a decision function $\mathcal{G}(\cdot)$:

$$\mathcal{G}(\mathbf{x}) = \begin{cases} \text{in} & \mathcal{S}(\mathbf{x}) > \gamma, \\ \text{out} & \mathcal{S}(\mathbf{x}) < \gamma. \end{cases} \quad (1)$$

where \mathbf{x} denotes the data encountered at the inference stage, $\mathcal{S}(\cdot)$ is the seeking scoring function, and γ is a chosen threshold to make a large portion of ID data correctly classified (e.g., 95%). The difficulty of OOD detection lies

in designing an appropriate scoring function $\mathcal{S}(\cdot)$ such that the score distributions of ID and OOD data overlap as little as possible.

3.2 RankFeat: Rank-1 Feature Removal

Consider the reshaped high-level feature map $\mathbf{X} \in \mathbb{R}^{C \times HW}$ of a deep network (the batch size is omitted for simplicity). Here ‘high-level feature’ denotes the feature map that carries rich semantics in the later layers of a network (e.g., the output of Block 3 or Block 4 of a typical deep model like ResNet). Our RankFeat first performs the Singular Value Decomposition (SVD) on each individual feature matrix in the mini-batch to decompose the feature:

$$\mathbf{X} = \mathbf{U}\mathbf{S}\mathbf{V}^T \quad (2)$$

where $\mathbf{S} \in \mathbb{R}^{C \times HW}$ is the rectangular diagonal singular value matrix, and $\mathbf{U} \in \mathbb{R}^{C \times C}$ and $\mathbf{V} \in \mathbb{R}^{HW \times HW}$ are left and right orthogonal singular vector matrices, respectively. Then RankFeat removes the rank-1 matrix from the feature as:

$$\mathbf{X}' = \mathbf{X} - \mathbf{s}_1 \mathbf{u}_1 \mathbf{v}_1^T \quad (3)$$

where \mathbf{s}_1 is the largest singular value, and \mathbf{u}_1 and \mathbf{v}_1 are the corresponding left and right singular vectors, respectively. The perturbed feature is fed into the rest of the network to generate the logit predictions \mathbf{y}' . Finally, RankFeat computes the energy score of the logits for the input \mathbf{x} as:

$$\text{RankFeat}(\mathbf{x}) = \log \sum \exp(\mathbf{y}') \quad (4)$$

By removing the rank-1 matrix composed by the dominant singular value \mathbf{s}_1 , the over-confident predictions of OOD data are largely perturbed. In contrast, the decisions of ID data are mildly influenced. This could help to separate the ID and OOD data better in the logit space.

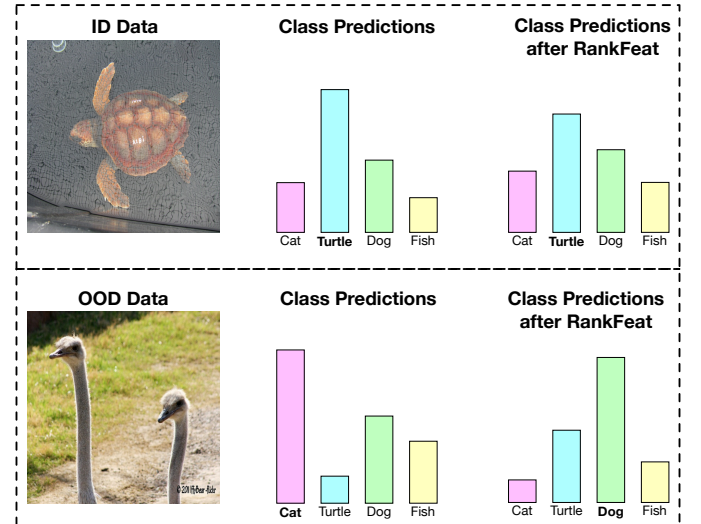


Fig. 4: Impact of RankFeat on the class predictions of ID and OOD data. The class predictions of OOD data are significantly more perturbed than those of ID data.

Fig. 4 gives an intuitive example of how the class predictions are impacted by our RankFeat. For the ID data, the class predictions are only mildly influenced; the same category is predicted correctly. By contrast, the logit distribution of OOD data is significantly perturbed, and the predicted category is inconsistent after performing RankFeat.

3.2.1 Acceleration by Power Iteration

Since RankFeat only involves the dominant singular value and vectors, there is no need to compute the full SVD of the feature matrix. Hence our method can be potentially accelerated by Power Iteration (PI). The PI algorithm is originally used to approximate the dominant eigenvector of a Hermitian matrix. With a slight modification, it can also be applied to general rectangular matrices. Given the feature \mathbf{X} , the modified PI takes the coupled iterative update:

$$\mathbf{v}_k = \frac{\mathbf{X}\mathbf{u}_k}{\|\mathbf{X}\mathbf{u}_k\|}, \mathbf{u}_{k+1} = \left(\frac{\mathbf{v}_k^T \mathbf{X}}{\|\mathbf{v}_k^T \mathbf{X}\|} \right)^T \quad (5)$$

where \mathbf{u}_0 and \mathbf{v}_0 are initialized with random orthogonal vectors and converge to the left and right singular vectors, respectively. After certain iterations, the dominant singular value is computed as $s_1 = \mathbf{v}_k^T \mathbf{X} \mathbf{u}_k$. As will be illustrated in Sec. 5.3.4, the approximate solution computed by PI achieves very competitive performance against the SVD but yields much less time overhead.

3.2.2 Combination of Multi-scale Features

Our RankFeat works at various later depths of a model, *i.e.*, Block 3 and Block 4. Since intermediate features might focus on different semantic information, their decision cues are very likely to be different. It is thus natural to consider fusing the scores to leverage the distinguishable information of both features for further performance improvements. Let \mathbf{y}' and \mathbf{y}'' denote the logit predictions of Block 3 and Block 4 features, respectively. RankFeat performs the fusion at the logit space and computes the score function as $\log \sum \exp((\mathbf{y}' + \mathbf{y}'')/2)$. Different fusion strategies will be explored in Sec. 5.3.5.

3.3 RankWeight: Rank-1 Weight Removal

The impressive performance of RankFeat indicates that the over-confidence of OOD samples is related to the rank-1 feature map composed by the dominant singular pairs. A natural question is *can we observe similar behaviors in other aspects of deep models and further leverage the abnormality for OOD detection?* We investigate this research question and find that the rank-1 parameter matrix also has a significant impact on the decisions of OOD data. We propose our RankWeight which similarly removes the rank-1 weight from the parameter matrices of the deep layer.

Let \mathbf{M} denote the parameter matrix at the deep layer which generates the high-level feature map \mathbf{X} in Eq. (2). In convolution neural networks \mathbf{M} refers to the weights of convolution kernels, while \mathbf{M} represents the weights of fully-connected layers in Transformers. Similar to Eqs. (2) and (3), we first perform SVD on the weights and remove the rank-1 matrix from the parameter as:

$$\mathbf{M}' = \mathbf{M} - \tilde{s}_1 \tilde{\mathbf{u}}_1 \tilde{\mathbf{v}}_1^T \quad (6)$$

where \tilde{s}_1 , $\tilde{\mathbf{u}}_1$, and $\tilde{\mathbf{v}}_1$ are the dominant singular value and vectors of \mathbf{M} . For a given input \mathbf{x} , the model with perturbed parameters \mathbf{M}' predicts the logits $\tilde{\mathbf{y}}$. We compute the score function as:

$$\text{RankWeight}(\mathbf{x}) = \log \sum \exp(\tilde{\mathbf{y}}) \quad (7)$$

Our method prunes the weights that are likely to cause the over-confidence of OOD samples. As can be seen in Fig. 1(c),

the pruning procedure has a slight impact on ID data but drastically perturbs the predictions of OOD samples. The ID and OOD data are thus easier to separate in the logit space.

3.3.1 Layers to Prune

We perform RankWeight **at the last parametric layer before the fully-connected layer** of the model, *i.e.*, the last convolution layer for convolution networks or the linear layer of the last MLP for Transformers. We find that it is sufficient to prune the parameters of **only one layer** in the model using RankWeight. As will be illustrated in Sec. 5.3.6, pruning more layers would negatively influence the performance. This observation might also indicate that the over-confidence of OOD samples happens more in the deep layers.

3.3.2 No Incurred Time Costs

Our RankWeight only requires computing the SVD of the parameter matrices once during the test stage. The time cost is negligible compared to classifying the whole ID dataset and multiple OOD test sets. Therefore, it almost does not incur any additional time costs to the standard inference procedure. In practice, the computational cost for each sample is the same as a single forward pass.

3.3.3 Combination with RankFeat

Our RankWeight can be further combined with RankFeat to perform joint OOD detection. That is, we simultaneously remove the rank-1 matrix from both the high-level feature and the deep parameter matrix. These two methods complement each other and eliminate the over-confidence originating from the feature and the parameters.

3.3.4 Compatibility with Other OOD Approaches

Notably, our RankWeight can be incorporated with a wide range of OOD detection methods, including GradNorm [3], ReAct [6], ASH [18], and VRA [26]. As will be discussed in Sec. 5.2.5, the integration of RankWeight would further boost the performance of these methods by a large margin of **18.83%** in FPR95 on average.

Notice that our RankWeight simply perturbs the model weights of one layer, which is not data-aware. The standalone use of RankWeight has competitive performance on different benchmarks. Only when integrated into data-aware OOD detection methods as a plugin, it can boost the performance of other methods to new *state-of-the-art*.

4 THEORETICAL ANALYSIS

In this section, we perform some theoretical analyses on RankFeat and RankWeight to support the empirical results. We start by proving that removing the rank-1 feature with a larger s_1 would reduce the upper bound of RankFeat score more. Then based on Random Matrix Theory (RMT), we show that removing the rank-1 matrix makes the statistics of OOD features closer to random matrices. Subsequently, the theoretical connection of ReAct and our RankFeat is analyzed and discussed: both approaches work by optimizing the score upper bound determined by s_1 . ReAct manually uses a pre-defined threshold to clip the term with s_1 , whereas our RankFeat directly optimizes the bound by subtracting this term. Finally, we show our RankWeight can tighten the upper bound and make our bound analysis more practical.

4.1 RankFeat Reduces Upper Bounds of OOD Data More

For our RankFeat score function, we can express its upper bound in an analytical form. Moreover, the upper bound analysis explicitly indicates that removing the rank-1 matrix with a larger first singular value would reduce the upper bound more. Specifically, we have the following proposition.

Proposition 1. *The upper bound of RankFeat score is defined as $\text{RankFeat}(\mathbf{x}) < \frac{1}{HW} \left(\sum_{i=1}^N \mathbf{s}_i - \mathbf{s}_1 \right) \|\mathbf{W}\|_\infty + \|\mathbf{b}\|_\infty + \log(Q)$ where Q denotes the number of categories, and \mathbf{W} and \mathbf{b} are the weight and bias of the last layer, respectively. A larger \mathbf{s}_1 would reduce the upper bound more.*

Proof. For the feature $\mathbf{X} \in \mathbb{R}^{C \times HW}$, its SVD $\mathbf{U}\mathbf{S}\mathbf{V}^T = \mathbf{X}$ can be expressed as the summation of rank-1 matrices $\mathbf{X} = \sum \mathbf{s}_i \mathbf{u}_i \mathbf{v}_i^T$. The feature perturbed by RankFeat can be computed as:

$$\mathbf{X}' = \mathbf{X} - \mathbf{s}_1 \mathbf{u}_1 \mathbf{v}_1^T = \sum_{i=2}^N \mathbf{s}_i \mathbf{u}_i \mathbf{v}_i^T \quad (8)$$

where N denotes the shorter side of the matrix (usually $N=HW$). In most deep models [25], [81], usually the last feature map needs to pass a Global Average Pooling (GAP) layer to collapse the width and height dimensions. The GAP layer can be represented by a vector

$$\mathbf{m} = \frac{1}{HW} [1, 1, \dots, 1]^T \quad (9)$$

The pooled feature map is calculated as $\mathbf{X}'\mathbf{m}$. Then the output logits are computed by the matrix-vector product with the classification head as:

$$\mathbf{y}' = \mathbf{W}\mathbf{X}'\mathbf{m} + \mathbf{b} = \sum_{i=2}^N (\mathbf{s}_i \mathbf{W}\mathbf{u}_i \mathbf{v}_i^T \mathbf{m}) + \mathbf{b} \quad (10)$$

where $\mathbf{W} \in \mathbb{R}^{W \times C}$ denotes the weight matrix, $\mathbf{b} \in \mathbb{R}^{Q \times 1}$ represents the bias vector, and $\mathbf{y}' \in \mathbb{R}^{Q \times 1}$ is the output logits that correspond to the perturbed feature \mathbf{X}' . Our RankFeat score is computed as:

$$\text{RankFeat}(\mathbf{x}) = \log \sum_{i=1}^Q \exp(\mathbf{y}'_i) \quad (11)$$

where \mathbf{x} is the input image, and Q denotes the number of categories. Here we choose Energy [27] as the base function due to its theoretical alignment with the input probability density and its strong empirical performance. Eq. (11) can be re-formulated by the Log-Sum-Exp trick

$$\log \sum_{i=1}^Q \exp(\mathbf{y}'_i) = \log \sum_{i=1}^Q \exp(\mathbf{y}'_i - \max(\mathbf{y}')) + \max(\mathbf{y}') \quad (12)$$

The above equation directly yields the tight bound as:

$$\max(\mathbf{y}') < \log \sum \exp(\mathbf{y}') < \max(\mathbf{y}') + \log(Q) \quad (13)$$

Since $\max(\mathbf{y}') \leq \max(|\mathbf{y}'|) = \|\mathbf{y}'\|_\infty$, we have

$$\begin{aligned} \text{RankFeat}(\mathbf{x}) &= \log \sum \exp(\mathbf{y}') \\ &< \max(\mathbf{y}') + \log(Q) \\ &\leq \|\mathbf{y}'\|_\infty + \log(Q) \end{aligned} \quad (14)$$

The vector norm has the property of triangular inequality, i.e., $\|\mathbf{a} + \mathbf{c}\| \leq \|\mathbf{a}\| + \|\mathbf{c}\|$ holds for any vectors \mathbf{a} and \mathbf{c} . Moreover, since both \mathbf{u} and \mathbf{v} are orthogonal vectors, we have the relation $\|\mathbf{u}_i\|_\infty \leq 1$ and $\|\mathbf{v}_i\|_\infty \leq 1$. Relying on these two properties, injecting eq. (10) into eq. (14) leads to

$$\begin{aligned} \text{RankFeat}(\mathbf{x}) &< \sum_{i=2}^N \mathbf{s}_i \|\mathbf{W}\mathbf{u}_i \mathbf{v}_i^T \mathbf{m}\|_\infty + \|\mathbf{b}\|_\infty + \log(Q) \\ &\leq \sum_{i=2}^N \mathbf{s}_i \|\mathbf{W}\mathbf{m}\|_\infty + \|\mathbf{b}\|_\infty + \log(Q) \end{aligned} \quad (15)$$

Since \mathbf{m} is a scaled all-ones vector, we have $\|\mathbf{W}\mathbf{m}\|_\infty = \|\mathbf{W}\|_\infty / HW$. The bound is simplified as:

$$\text{RankFeat}(\mathbf{x}) < \frac{1}{HW} \left(\sum_{i=1}^N \mathbf{s}_i - \mathbf{s}_1 \right) \|\mathbf{W}\|_\infty + \|\mathbf{b}\|_\infty + \log(Q) \quad (16)$$

As indicated above, removing a larger \mathbf{s}_1 would reduce the upper bound of RankFeat score more. \square

Remark: Considering that OOD feature usually has a much larger \mathbf{s}_1 (see Fig. 1(a)), RankFeat would reduce the upper bound of OOD samples more and amplify the upper bound gap between ID and OOD data.

Notice that our bound analysis strives to improve the understanding of OOD methods from new perspectives instead of giving a strict guarantee of the score. For example, the upper bound can be used to explain the shrinkage and skew of score distributions in Fig. 3. Subtracting \mathbf{s}_1 would largely reduce the numerical range of both ID and OOD scores, which could squeeze score distributions. Since the dominant singular value \mathbf{s}_1 contributes most to the score, removing \mathbf{s}_1 is likely to make many samples have similar scores. This would concentrate samples in a smaller region and further skew the distribution. Given that the OOD feature tends to have a much larger \mathbf{s}_1 , this would have a greater impact on OOD data and skew the OOD score distribution more.

Remark: Though we use the assumption of GAP in Prop. 1, this assumption is not really necessary for deriving our upper bounds. For example, when the model is Vision Transformer which does not have any pooling layer, the upper bounds still hold — the only difference is that the pooling vector \mathbf{m} will be removed in the bounds:

$$\begin{aligned} \text{RankFeat}(\mathbf{x}) &< \sum_{i=2}^N \mathbf{s}_i \|\mathbf{W}\mathbf{u}_i \mathbf{v}_i^T \mathbf{m}\|_\infty + \|\mathbf{b}\|_\infty + \log(Q) \\ &\leq \sum_{i=2}^N \mathbf{s}_i \|\mathbf{W}\mathbf{m}\|_\infty + \|\mathbf{b}\|_\infty + \log(Q) \\ &= \frac{1}{HW} \left(\sum_{i=1}^N \mathbf{s}_i - \mathbf{s}_1 \right) \|\mathbf{W}\|_\infty + \|\mathbf{b}\|_\infty + \log(Q) \end{aligned} \quad (17)$$

As indicated above, the upper bounds of our RankFeat hold for general neural networks with fully connected layers.

4.2 Removing Rank-1 Matrix Makes the Statistics of OOD Features Closer to Random Matrices

Now we turn to use RMT to analyze the statistics of OOD and ID feature matrices. For a random matrix of a given shape,

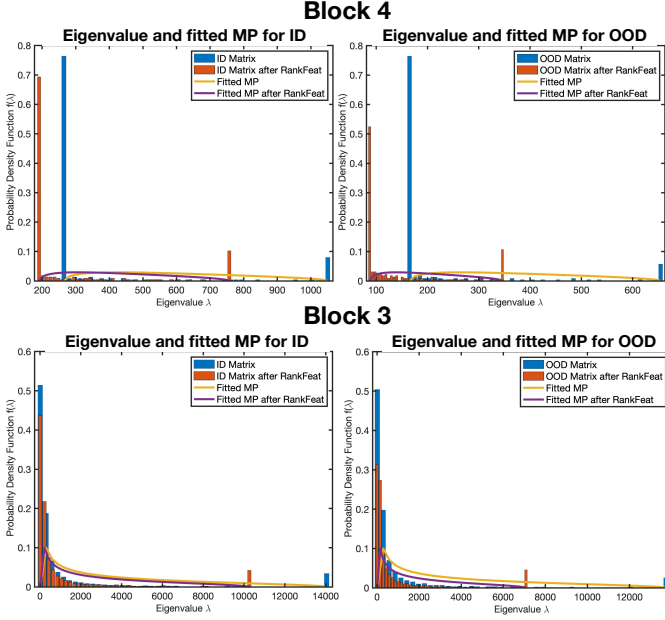


Fig. 5: The exemplary eigenvalue distribution of ID/OOD feature and the fitted MP distribution. After the rank-1 matrix is removed, the lowest bin of OOD feature has a larger reduction and the middle bins gain some growth, making the OOD feature statistics closer to the MP distribution.

the density of its eigenvalue asymptotically converges to the Manchenko-Pastur (MP) distribution [82], [83]. Formally, we have the following theorem:

Theorem 1 (Manchenko-Pastur Law [82], [83]). *Let \mathbf{X} be a random matrix of shape $t \times n$ whose entries are random variables with $E(\mathbf{X}_{ij}) = 0$ and $E(\mathbf{X}_{ij}^2) = 1$. Then the eigenvalues of the sample covariance $\mathbf{Y} = \frac{1}{n}\mathbf{X}\mathbf{X}^T$ converges to the probability density function: $\rho(\lambda) = \frac{t}{n} \frac{\sqrt{(\lambda_+ - \lambda)(\lambda - \lambda_-)}}{2\pi\lambda\sigma^2}$ for $\lambda \in [\lambda_-, \lambda_+]$ where $\lambda_- = \sigma^2(1 - \sqrt{\frac{n}{t}})^2$ and $\lambda_+ = \sigma^2(1 + \sqrt{\frac{n}{t}})^2$.*

We leave the proof in Sec. E of the Supplementary Material. This theorem implies the possibility of measuring the statistical distance between ID/OOD features and random matrices. To compute the statistical distance, we randomly sample 1,000 ID and OOD feature matrices and compute the KL divergence between the actual eigenvalue distribution and the fitted MP distribution.

Fig. 5 and Table 2 present the exemplary eigenvalue distribution and the average evaluation results of Block 4 and Block 3 features, respectively. For the original feature, the OOD and ID feature matrices exhibit similar behaviors: the distances to the fitted MP distribution are roughly the same ($diff \approx 0.1$). However, when we perform RankFeat or RankWeight, i.e., removing the rank-1 feature or parameter, the OOD feature matrix has a much larger drop in the KL divergence. This indicates that removing the rank-1 matrix makes the statistics of the OOD feature closer to random matrices, i.e., the OOD feature is very likely to become less informative than the ID feature. The result partly explains the working mechanism of RankFeat and RankWeight: by removing the feature matrix or the parameter matrix where OOD data might convey more information than ID data, the two distributions have a larger discrepancy and can be better separated.

4.3 Connection between RankFeat and ReAct [6]

ReAct clips the activations at the penultimate layer of a model to distinguish ID and OOD samples. Given the feature \mathbf{X} and the pooling layer \mathbf{m} , the perturbation can be defined as:

$$\min(\mathbf{X}\mathbf{m}, \tau) = \mathbf{X}\mathbf{m} - \max(\mathbf{X}\mathbf{m} - \tau, 0) \quad (18)$$

where τ is a pre-defined threshold. Their method shares some similarity with RankFeat formulation $\mathbf{X}\mathbf{m} - \mathbf{s}_1\mathbf{u}_1\mathbf{v}_1^T\mathbf{m}$. Both approaches subtract from the feature a portion of information that is most likely to cause the over-confidence of OOD prediction. ReAct selects the manually-defined threshold τ based on statistics of the whole ID set, while RankFeat generates the structured rank-1 matrix from the feature itself. Taking a step further, ReAct has the score inequality following eq. (14)

$$\text{ReAct}(\mathbf{x}) < \|\mathbf{W}\mathbf{X}\mathbf{m} - \mathbf{W}\max(\mathbf{X}\mathbf{m} - \tau, 0)\|_\infty + \|\mathbf{b}\|_\infty + \log(Q) \quad (19)$$

Since \mathbf{X} is non-negative (output of ReLU), we have $\max(\mathbf{X}\mathbf{m}) \geq \max(\mathbf{X})/HW$. Exploiting the vector norm inequality $\|\mathbf{X}\|_F \geq \|\mathbf{X}\|_2$ leads to the relation $\max(\mathbf{X}) \geq s_1/\sqrt{CHW}$. Relying on this property, the above inequality can be re-formulated as:

$$\begin{aligned} \text{ReAct}(\mathbf{x}) &< \frac{1}{HW} \sum_{i=1}^N s_i \|\mathbf{W}\|_\infty \\ &- \boxed{\frac{1}{HW} \max\left(\frac{s_1}{\sqrt{CHW}} - \tau, 0\right) \|\mathbf{W}\|_\infty} + \|\mathbf{b}\|_\infty + \log(Q) \end{aligned} \quad (20)$$

As indicated above, the upper bound of ReAct is also determined by the largest singular value s_1 . In contrast, the upper bound of our RankFeat can be expressed as:

$$\begin{aligned} \text{RankFeat}(\mathbf{x}) &< \frac{1}{HW} \sum_{i=1}^N s_i \|\mathbf{W}\|_\infty \\ &- \boxed{\frac{1}{HW} s_1 \|\mathbf{W}\|_\infty} + \|\mathbf{b}\|_\infty + \log(Q) \end{aligned} \quad (21)$$

The upper bounds of both methods resemble each other with the only different term boxed. From this point of view, both methods distinguish the ID and OOD data by eliminating the impact of the term containing s_1 in the upper bound. ReAct optimizes it by clipping the term with a manually-defined threshold, which is indirect and might be sub-optimal. Moreover, the threshold selection requires statistics of the whole ID set. In contrast, our RankFeat does not require any extra data and directly subtracts this underlying term which is likely to cause the over-confidence of OOD samples.

4.4 RankWeight Tightens the Upper Bounds

Given the parameter matrix \mathbf{M} and the feature \mathbf{X}_{L-1} before this layer, we generate the target high-level feature as:

$$\mathbf{X}_L = \mathbf{M}\mathbf{X}_{L-1} \quad (22)$$

where \mathbf{X}_L corresponds to the feature \mathbf{X} in the bound analysis of Eq. (8), and the bias is neglected for simplicity. The above equation holds for linear layers in Transformers and also convolution layers in CNNs (convolutional kernels can be extended to circular Toeplitz matrices for matrix

TABLE 1: Main results on ResNetv2-101 [81]. All values are reported in percentages, and these *post hoc* methods are directly applied to the model pre-trained on ImageNet-1k [84]. The best four results are highlighted with **red**, **blue**, **cyan**, and **brown**.

Methods	iNaturalist		SUN		Places		Textures		Average	
	FPR95 (↓)	AUROC (↑)	FPR95 (↓)	AUROC (↑)	FPR95 (↓)	AUROC (↑)	FPR95 (↓)	AUROC (↑)	FPR95 (↓)	AUROC (↑)
MSP [85]	63.69	87.59	79.89	78.34	81.44	76.76	82.73	74.45	76.96	79.29
ODIN [38]	62.69	89.36	71.67	83.92	76.27	80.67	81.31	76.30	72.99	82.56
Energy [27]	64.91	88.48	65.33	85.32	73.02	81.37	80.87	75.79	71.03	82.74
Mahalanobis [24]	96.34	46.33	88.43	65.20	89.75	64.46	52.23	72.10	81.69	62.02
GradNorm [3]	50.03	90.33	46.48	89.03	60.86	84.82	61.42	81.07	54.70	86.71
ReAct [6]	44.52	91.81	52.71	90.16	62.66	87.83	70.73	76.85	57.66	86.67
RankFeat (Block 4)	46.54	81.49	27.88	92.18	38.26	88.34	46.06	89.33	39.69	87.84
RankFeat (Block 3)	49.61	91.42	39.91	92.01	51.82	88.32	41.84	91.44	45.80	90.80
RankFeat (Block 3 + 4)	41.31	91.91	29.27	94.07	39.34	90.93	37.29	91.70	36.80	92.15
RankWeight	45.96	92.29	45.51	90.89	52.12	88.23	68.28	81.54	52.95	88.24
RankFeat+RankWeight	12.97	96.01	10.64	97.46	15.64	96.30	25.27	95.01	16.13	96.20

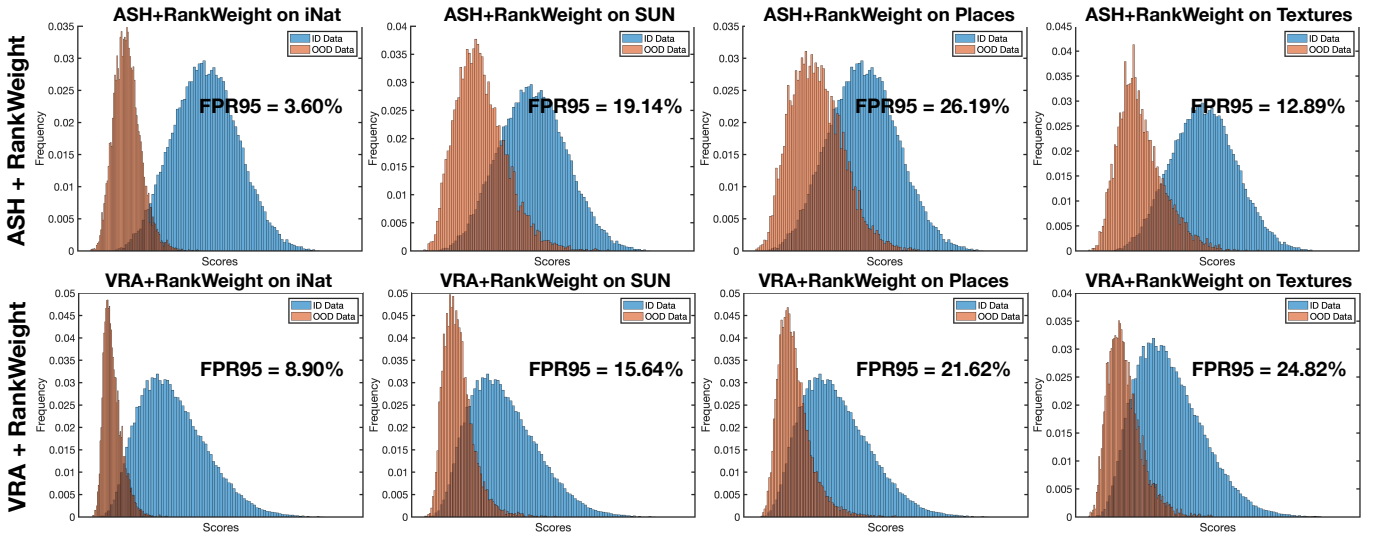


Fig. 6: Score distributions of some OOD detection [18], [26] approached integrated with our RankWeight on ResNetv2-101.

TABLE 2: The KL divergence between ID/OOD feature and the fitted MP distribution. When the rank-1 feature or the rank-1 parameter is removed, the statistics of OOD matrix are closer to random matrices.

Matrix Type	Block 4		Block 3	
	ID	OOD	ID	OOD
Original feature matrix	18.36	18.24	11.27	11.18
Removing rank-1 feature	17.07 (↓ 1.29)	15.79 (↓ 2.45)	9.84 (↓ 1.45)	8.71 (↓ 2.47)
Removing rank-1 weight	15.34 (↓ 3.02)	13.98 (↓ 4.26)	8.52 (↓ 2.75)	6.79 (↓ 4.39)

multiplication). When our RankWeight is performed, the feature would become:

$$\mathbf{X}'_L = \mathbf{M}'\mathbf{X}_{L-1} = \mathbf{M}\mathbf{X}_{L-1} - \tilde{\mathbf{s}}_1\tilde{\mathbf{u}}_1\tilde{\mathbf{v}}_1^T\mathbf{X}_{L-1} \quad (23)$$

Let $\tilde{\mathbf{s}}_2$ denotes the second largest singular value of \mathbf{M} . Then according to the inequality $\sigma_i(\mathbf{AB}) \leq \sigma_{\max}(\mathbf{A})\sigma_i(\mathbf{B})$, the singular values of the new feature would satisfy:

$$\sigma_i(\mathbf{X}'_L) \leq \tilde{\mathbf{s}}_2\sigma_i(\mathbf{X}_{L-1}) \quad (24)$$

where $\sigma_i(\cdot)$ denote the i -th singular value. Notice that for the original feature \mathbf{X}_L , the singular values have:

$$\mathbf{s}_i = \sigma_i(\mathbf{X}_L) \leq \tilde{\mathbf{s}}_1\sigma_i(\mathbf{X}_{L-1}) \quad (25)$$

We can write the upper bound of RankWeight as:

$$\begin{aligned} \text{RankWeight}(\mathbf{x}) &\leq \frac{\sum_{i=1}^N \sigma_i(\mathbf{X}'_L)}{HW} \|\mathbf{W}\|_\infty + C \\ &\leq \frac{\sum_{i=1}^N \tilde{\mathbf{s}}_2\sigma_i(\mathbf{X}_{L-1})}{HW} \|\mathbf{W}\|_\infty + C \\ &= \frac{\tilde{\mathbf{s}}_2}{\tilde{\mathbf{s}}_1} \frac{\sum_{i=1}^N \tilde{\mathbf{s}}_1\sigma_i(\mathbf{X}_{L-1})}{HW} \|\mathbf{W}\|_\infty + C \end{aligned} \quad (26)$$

Here we use C to represent the constants $\|\mathbf{b}\|_\infty + \log(Q)$. Recall that for the Energy score, the upper bound is:

$$\text{Energy}(\mathbf{x}) \leq \frac{\sum_{i=1}^N \tilde{\mathbf{s}}_1\sigma_i(\mathbf{X}_{L-1})}{HW} \|\mathbf{W}\|_\infty + C \quad (27)$$

Since we have $\tilde{\mathbf{s}}_2/\tilde{\mathbf{s}}_1 \leq 1$, it is clear that our RankWeight tightens the upper bound of the Energy score. Similarly, when RankWeight is combined with RankFeat or ReAct,

TABLE 3: The evaluation results on SqueezeNet [86], T2T-ViT-24 [87], ViT-B/16 [88], and Swin-B [89]. All values are reported in percentages, and these *post hoc* methods are directly applied to the model pre-trained on ImageNet-1k [84]. The best four results are highlighted with **red**, **blue**, **cyan**, and **brown**. On Swin-B [89], since the Energy score does not achieve reasonable performance, we select MSP as the base method for integrating our RankFeat and RankWeight.

Model	Methods	iNaturalist		SUN		Places		Textures		Average	
		FPR95 (↓)	AUROC (↑)	FPR95 (↓)	AUROC (↑)	FPR95 (↓)	AUROC (↑)	FPR95 (↓)	AUROC (↑)	FPR95 (↓)	AUROC (↑)
SqueezeNet [86]	MSP [85]	89.83	65.41	83.03	72.25	87.27	67.00	94.61	41.84	88.84	61.63
	ODIN [38]	90.79	65.75	78.32	78.37	83.23	73.31	92.25	43.43	86.15	65.17
	Energy [27]	79.27	73.30	56.41	87.88	67.74	82.73	67.16	64.51	67.65	77.11
	Mahalanobis [24]	91.50	51.79	90.33	62.18	92.26	56.63	58.60	67.16	83.17	59.44
	GradNorm [3]	76.31	73.92	53.63	87.55	65.99	83.28	68.72	68.07	66.16	78.21
	ReAct [6]	76.78	68.56	87.57	66.37	88.80	66.20	51.05	76.57	76.05	69.43
	RankFeat (Block 4)	61.67	83.09	46.72	88.31	61.31	80.52	38.04	88.82	51.94	85.19
	RankFeat (Block 3)	71.04	81.50	49.18	90.43	62.94	85.82	50.14	79.32	58.33	84.28
	RankFeat (Block 3 + 4)	65.81	83.06	46.64	90.17	61.56	84.51	42.54	85.00	54.14	85.69
	RankWeight	77.91	62.77	44.03	89.89	58.35	84.11	61.75	66.26	60.51	75.76
T2T-ViT-24 [87]	RankFeat+RankWeight	53.18	87.46	39.21	91.55	54.88	85.39	33.89	91.07	45.29	88.87
	MSP [85]	48.92	88.95	61.77	81.37	69.54	80.03	62.91	82.31	60.79	83.17
	ODIN [38]	44.07	88.17	63.83	78.46	68.19	75.33	54.27	83.63	57.59	81.40
	Energy [27]	52.95	82.93	68.55	73.06	74.24	68.17	51.05	83.25	61.70	76.85
	Mahalanobis [24]	90.50	58.13	91.71	50.52	93.32	49.60	80.67	64.06	89.05	55.58
	GradNorm [3]	99.30	25.86	98.37	28.06	99.01	25.71	92.68	38.80	97.34	29.61
	ReAct [6]	52.17	89.51	65.23	81.03	68.93	78.20	52.54	85.46	59.72	83.55
	RankFeat	50.27	87.81	57.18	84.33	66.22	80.89	32.64	89.36	51.58	85.60
	RankWeight	22.54	94.27	61.76	79.86	63.28	77.39	44.11	86.66	47.92	84.55
	RankFeat+RankWeight	20.36	95.52	47.33	88.48	55.39	85.74	27.48	90.65	37.64	90.10
ViT-B/16 [88]	MSP [85]	47.96	88.57	69.55	78.95	71.15	77.96	63.76	79.84	63.11	81.33
	ODIN [38]	46.13	87.33	68.70	74.67	70.68	72.65	62.11	77.02	61.91	77.92
	Energy [27]	63.30	80.89	76.80	68.00	77.87	65.47	67.06	73.76	71.26	72.03
	Mahalanobis [24]	98.95	25.49	93.18	56.67	92.56	58.07	89.50	54.70	93.55	48.73
	GradNorm [3]	89.92	54.41	96.02	41.89	96.30	39.61	91.79	47.04	93.51	45.74
	ReAct [6]	72.99	81.77	79.29	73.42	79.22	71.72	67.98	77.85	74.87	76.19
	RankFeat	62.90	88.18	61.51	83.53	63.14	81.51	55.46	85.35	60.75	84.64
	RankWeight	70.45	77.09	78.31	68.05	79.19	66.36	62.80	77.68	72.69	72.30
	RankFeat+RankWeight	48.93	90.27	51.85	86.58	53.33	84.81	49.68	87.81	50.95	87.37
Swin-B [89]	MSP [85]	52.81	85.06	71.50	76.48	71.35	77.11	76.54	67.16	68.05	76.45
	ODIN [38]	58.06	81.49	72.22	72.73	71.82	73.74	79.26	61.63	70.34	72.40
	Energy [27]	86.85	65.09	83.54	63.38	82.80	64.86	89.13	51.31	85.58	61.16
	Mahalanobis [24]	94.92	63.64	95.44	46.11	94.18	47.26	79.68	65.63	91.06	55.66
	GradNorm [3]	97.43	31.61	94.08	36.89	94.02	38.73	95.48	30.37	95.25	34.40
	ReAct [6]	80.93	77.32	79.32	72.05	78.96	72.71	83.90	63.64	80.78	71.43
	RankFeat*	51.38	87.66	60.32	84.52	64.77	82.29	72.36	81.04	62.21	83.88
	RankWeight*	49.14	87.89	67.24	81.18	67.75	81.68	74.04	71.90	64.54	80.66
	RankFeat+RankWeight*	39.64	90.32	58.47	85.57	62.87	82.89	48.28	87.72	52.32	86.63

we see the upper bound is also scaled by a factor of $\tilde{s}_2/\tilde{s}_1 \leq 1$. Specifically, for RankFeat we have:

$$\text{RankWeight}(\mathbf{x}) + \text{RankFeat}(\mathbf{x}) \leq \frac{\tilde{s}_2}{\tilde{s}_1} \frac{1}{HW} \left(\sum_{i=1}^N \mathbf{s}_i - \mathbf{s}_1 \right) \|\mathbf{W}\|_\infty + \|\mathbf{b}\|_\infty + \log(Q) \quad (28)$$

For ReAct, we have:

$$\text{RankWeight}(\mathbf{x}) + \text{ReAct}(\mathbf{x}) \leq \frac{\tilde{s}_2}{\tilde{s}_1} \frac{1}{HW} \left(\sum_{i=1}^N \mathbf{s}_i - \max \left(\frac{\mathbf{s}_1}{\sqrt{CHW}} - \tau, 0 \right) \right) \|\mathbf{W}\|_\infty + \|\mathbf{b}\|_\infty + \log(Q) \quad (29)$$

In a nutshell, our RankWeight re-scales the singular values of the upper bound, thus making the bound tighter and the associated analysis more practically useful.

5 EXPERIMENTAL RESULTS

In this section, we first discuss the setup in Sec. 5.1, and then present the main large-scale experimental results in Sec. 5.2, followed by the extensive ablation studies in Sec. 5.3.

5.1 Setup

Datasets. In line with [3], [6], [60], we mainly evaluate our method on the large-scale ImageNet-1k benchmark [84]. The large-scale dataset is more challenging than the traditional CIFAR benchmark [90] because the images are more realistic and diverse (*i.e.*, 1.28M images of 1,000 classes). For the OOD datasets, we select four testsets from subsets of iNaturalist [91], SUN [92], Places [93], and Textures [94]. These datasets are crafted by [60] with non-overlapping categories from ImageNet-1k. Besides these four

TABLE 4: Comparisons on ResNetv2-101 [81] of some OOD detection approaches empowered by our RankWeight. Our RankWeight brings about consistent performance gain on all the testsets for every baseline.

Methods	iNaturalist		SUN		Places		Textures		Average	
	FPR95 (↓)	AUROC (↑)	FPR95 (↓)	AUROC (↑)	FPR95 (↓)	AUROC (↑)	FPR95 (↓)	AUROC (↑)	FPR95 (↓)	AUROC (↑)
GradNorm [3]	50.03	90.33	46.48	89.03	60.86	84.82	61.42	81.07	54.70	86.71
GradNorm [3] + RankWeight	15.53	97.44	20.58	96.55	26.26	95.53	57.57	86.39	29.99 (↑ 24.71)	93.93 (↑ 7.22)
ReAct [6]	44.52	91.81	52.71	90.16	62.66	87.83	70.73	76.85	57.66	86.67
ReAct [6] + RankWeight	20.42	96.53	31.99	94.84	37.67	93.37	54.40	84.75	36.12 (↑ 21.54)	92.37 (↑ 5.70)
VRA [26]	20.81	97.70	32.89	92.68	45.83	90.01	23.88	95.43	30.85	93.71
VRA [26]+ RankWeight	8.90	98.37	15.64	96.99	21.62	95.85	24.82	95.16	17.75 (↑ 13.10)	96.59 (↑ 2.88)
ASH [18]	21.22	96.37	38.42	90.85	51.37	88.10	14.73	97.19	31.44	93.13
ASH [18]+ RankWeight	3.60	99.07	19.14	96.45	26.19	95.46	12.89	97.57	15.46 (↑ 15.98)	97.13 (↑ 4.00)

OOD test sets, we further evaluate our method on the large-scale Species dataset. The Species [95] dataset is a large-scale OOD validation benchmark consisting of 71,3449 images, which is designed for ImageNet-1k [84] and ImageNet 21-k [96] as the ID sets. We select four sub-sets as the OOD benchmark, namely Protozoa, Microorganisms, Plants, and Mollusks. Besides the experiment on the large-scale benchmark, we also validate the effectiveness of our approach on the CIFAR [90] benchmark (see Sec. A of the Supplementary Material).

Baselines. We compare our method with 6 recent *post hoc* OOD detection methods, namely MSP [85], ODIN [38], Energy [27], Mahalanobis [24], GradNorm [3], and ReAct [6]. Also, we show that the two recent activation-shaping based approaches, *i.e.*, ASH [18] and VRA [26], can be further boosted by our RankWeight. The detailed illustration and settings are kindly referred to Sec. B of the Supplementary Material.

Architectures. In line with [3], the main evaluation is done using Google BiT-S model [96] pretrained on ImageNet-1k with ResNetv2-101 [81]. We also evaluate the performance on SqueezeNet [86], an alternative tiny architecture suitable for mobile devices, and on T2T-ViT-24 [87], a tokens-to-tokens vision transformer that has impressive performance when trained from scratch. We also benchmark our method on two other popular transformer architectures, *i.e.*, Vision Transformers (ViTs) [88] and SwinTransformer [89].

Implementation Details. At the inference stage, all the images are resized to 480×480 for ResNetv2-101 [81] and SqueezeNet [86]. The source codes are implemented with Pytorch 1.10.1, and all experiments are run on a single NVIDIA Quadro RTX 6000 GPU.

Evaluation Metrics. Following [3], [6], [60], we measure the performance using two main metrics: (1) the false positive rate (FPR95) of OOD examples when the true positive rate of ID samples is at 95%; and (2) the area under the receiver operating characteristic curve (AUROC).

Pseudo Code. Fig. 7 and 8 present the Pytorch-like implementation of our RankFeat and RankWeight, respectively. We use `torch.linalg.svd` to perform the SVD.

5.2 Results

```

1 #Our RankFeat (SVD) is applied on each individual \
2 #feature matrix within the mini-batch.
3 feat = model.features(inputs)
4 B, C, H, W = feat.size()
5 feat = feat.view(B, C, H * W)
6 u, s, vt = torch.linalg.svd(feat)
7 feat = feat - s[:,0:1].unsqueeze(2)*u[:, :,0:1].bmm(
8     vt[:,0:1,:])
9 feat = feat.view(B,C,H,W)
10 logits = model.classifier(feat)
11 score = torch.logsumexp(logits, dim=1)

```

Fig. 7: Pytorch-like codes of our RankFeat implementation.

```

1 weight = model.block4[-1].conv3.weight.data
2 u, s, vt = torch.linalg.svd(weight)
3 weight = weight - s[:,0:1].unsqueeze(2)*u[:, :,0:1].
4     bmm(vt[:,0:1,:])
5 model.block4[-1].conv3.weight.data = weight

```

Fig. 8: Pytorch-like codes of our RankWeight core implementation. Here we prune the last parameter matrix before the fully-connected layer by removing the rank-1 weight.

5.2.1 Main Results on ImageNet-1k

Following [3], the main evaluation is conducted using Google BiT-S model [96] pretrained on ImageNet-1k with ResNetv2-101 architecture [81]. Table 1 compares the performance of all the *post hoc* methods. For both Block 3 and Block 4 features, our RankFeat achieves impressive evaluation results across datasets and metrics. More specifically, RankFeat based on the Block 4 feature outperforms the previous best baseline by **15.01%** in the average FPR95, while the Block 3 feature-based RankFeat beats the previous best method by **4.09%** in the average AUROC. Their combination further surpasses other methods by **17.90%** in the average FPR95 and by **5.44%** in the average AUROC. The superior performances at various depths demonstrate the effectiveness and general applicability of RankFeat. The Block 3 feature has a higher AUROC but slightly falls behind the Block 4 feature in the FPR95, which can be considered a compromise between the two metrics. For our RankWeight, the evaluation results of its standalone usage are very competitive against previous baselines. Moreover, jointly using RankFeat and RankWeight establishes the new *state-of-the-art* of this benchmark, achieving a low FPR95 of **16.13%** and a high

TABLE 5: The evaluation results on four sub-sets of Species [95] based on ResNetv2-101 [81]. All values are reported in percentages, and these *post hoc* methods are directly applied to the model pre-trained on ImageNet-1k [84]. The best four results are highlighted with **red**, **blue**, **cyan**, and **brown**.

Methods	Protozoa		Microorganisms		Plants		Mollusks		Average	
	FPR95 (↓)	AUROC (↑)	FPR95 (↓)	AUROC (↑)	FPR95 (↓)	AUROC (↑)	FPR95 (↓)	AUROC (↑)	FPR95 (↓)	AUROC (↑)
MSP [85]	75.81	83.20	72.23	84.25	61.48	87.78	85.62	70.51	73.79	81.44
ODIN [38]	75.97	85.11	65.94	89.35	55.69	90.79	86.22	71.31	70.96	84.14
Energy [27]	79.49	84.34	60.87	90.30	54.67	90.95	88.47	70.53	70.88	84.03
ReAct [6]	81.74	84.26	58.82	85.88	36.90	93.78	90.58	76.33	67.02	85.06
RankFeat (Block 4)	66.98	70.19	39.06	86.67	46.31	79.98	80.14	59.92	58.12	74.19
RankFeat (Block 3)	58.99	88.81	49.72	90.04	47.01	91.85	80.37	79.61	59.02	87.58
RankFeat (Block 3 + 4)	52.78	88.65	37.21	92.82	38.07	92.88	76.38	78.13	51.11	88.37
RankWeight	47.49	92.10	29.94	95.23	24.76	95.79	65.32	84.32	41.88	91.86
RankFeat + RankWeight	27.57	92.55	14.17	96.19	9.51	97.67	37.94	86.58	22.30	93.25

TABLE 6: Comparison against training-needed methods on ImageNet-1k based on ResNetv2-101 [81].

Method	Post hoc?	Free of Validation Set?	FPR95 (↓)	AUROC (↑)
KL Matching [95]	✓	✗	54.30	80.82
MOS [60]	✗	✓	39.97	90.11
RankFeat	✓	✓	36.80	92.15
RankWeight	✓	✓	52.95	88.24
RankFeat+RankWeight	✓	✓	16.13	96.20

AUROC of **96.20%**. This implies that our RankFeat and RankWeight can complement each other to maximally separate and distinguish the ID and OOD data.

5.2.2 RankFeat/RankWeight Works on Alternative CNNs

Besides the experiment on ResNetv2 [81], we also evaluate our method on SqueezeNet [86], an alternative tiny network suitable for mobile devices and on-chip applications. This network is more challenging because the tiny network size makes the model prone to overfit the training data, which could increase the difficulty of distinguishing between ID and OOD samples. Table 3 top presents the performance of all the methods. Collectively, the performance of RankFeat and RankWeight is very competitive. Specifically, our RankFeat outperforms the previous best baseline by **14.22%** in FPR95 and by **7.48%** in AUROC, while our RankWeight surpasses the previous best method by **5.65%** in FPR95. When RankFeat and RankWeight are used simultaneously, the results achieve *state-of-the-art* performance, attaining a low FPR95 of **45.29%** and a high AUROC of **88.87%**.

5.2.3 RankFeat/RankWeight also Suits Transformers

To further demonstrate the applicability of our method, we evaluate RankFeat and RankWeight on Tokens-to-Tokens Vision Transformer (T2T-ViT) [87], Vision Transformers (ViTs) [88], and SwinTransformer [89]. Similar to the CNNs, our methods are performed on the final and penultimate tokens of T2T-ViT and ViT, respectively. Due to the sliding 7×7 window, the feature maps of SwinTransformer are small in dimensionality at the last layer; we hence perform our RankFeat and RankWeight on the third-to-last layer. Table 3 bottom compares the performance on T2T-ViT-24, ViT-B/16, and Swin-B. Our RankFeat outperforms the second-best method by **2.05%** in AUROC on T2T-ViT-24, by **3.31%** in

AUROC on ViT-B/16, and by **7.43%** in AUROC on Swin-B. Since the transformer models [87], [97] do not have increasing receptive fields like CNNs, we do not evaluate the performance at alternative network depths. When our RankWeight is applied, the FPR95 further reduces to **37.64%** and the AUROC increases to **90.10%** on T2T-ViT-24, the FPR95 further reduces to **50.95%** and the AUROC increases to **87.37%** on ViT-B/16, and the FPR95 further reduces to **52.32%** and the AUROC increases to **86.63%** on Swin-B. These experimental results indicate the flexible composability of our RankFeat and RankWeight on various Transformers.

TABLE 7: Ablation studies on keeping only the rank-1 matrix and removing the rank-n matrix.

Baselines	iNaturalist		SUN		Places		Textures		Average	
	FPR95 (↓)	AUROC (↑)	FPR95 (↓)	AUROC (↑)	FPR95 (↓)	AUROC (↑)	FPR95 (↓)	AUROC (↑)	FPR95 (↓)	AUROC (↑)
GradNorm [3]	50.03	90.33	46.48	89.03	60.86	84.82	61.42	81.07	54.70	86.71
ReAct [6]	44.52	91.81	52.71	90.16	62.66	87.83	70.73	76.85	57.66	86.67
Keeping Only Rank-1	48.97	91.93	62.63	84.62	72.42	79.79	49.42	88.86	58.49	86.30
Removing Rank-3	55.19	90.03	48.97	91.26	56.63	88.81	86.95	74.57	61.94	86.17
Removing Rank-2	50.04	89.30	48.55	90.99	56.23	88.38	76.86	81.37	57.92	87.51
Removing Rank-1	46.54	81.49	27.88	92.18	38.26	88.34	46.06	89.33	39.69	87.84

5.2.4 Comparison against Training-needed Approaches

Since our method is *post hoc*, we only compare it with other *post hoc* baselines. MOS [60] and KL Matching [95] are not taken into account because MOS needs extra training processes and KL Matching requires the labeled validation set to compute distributions for each class. Nonetheless, we note that our method can still hold an advantage against those approaches. Table 6 presents the average FPR95 and AUROC of these methods on the ImageNet-1k benchmark. Without any prior knowledge of the training or validation ID set, our RankFeat as well as its combination with RankWeight achieve better performance than previous training-needed approaches, outperforming previous methods by **23.84%** in average FPR95 and **6.09%**.

5.2.5 RankWeight Enhances Other OOD Approaches

Table 4 shows the performance of some OOD detection approaches incorporated with our RankWeight. Empowered by our method, each baseline gets consistent performance gain across different datasets with an average improvement

TABLE 8: Ablation studies on applying RankFeat to features at different network depths.

Layer	iNaturalist		SUN		Places		Textures		Average	
	FPR95 (↓)	AUROC (↑)	FPR95 (↓)	AUROC (↑)	FPR95 (↓)	AUROC (↑)	FPR95 (↓)	AUROC (↑)	FPR95 (↓)	AUROC (↑)
Block 1	87.81	77.00	59.15	87.29	65.50	84.35	94.15	60.41	76.65	77.26
Block 2	71.84	85.80	61.44	86.46	71.68	81.65	87.89	72.04	73.23	81.49
Block 3	49.61	91.42	39.91	92.01	51.82	88.32	41.84	91.44	45.80	90.80
Block 4	46.54	81.49	27.88	92.18	38.26	88.34	46.06	89.33	39.69	87.84

of **18.83%** in FPR95 and **4.95%** in AUROC. In particular, both VRA and ASH establish *state-of-the-art* performance when integrated with our RankWeight. The compatibility with a wide range of baselines demonstrates that our RankWeight serves as a general add-on for OOD detection methods.

5.2.6 Results on the Large-scale Species Dataset

We present the evaluation results on Species in Table 5. The results are coherent with our previous experiments on alternative benchmarks and architectures. Specifically, our RankFeat surpasses other methods by **15.91%** in the average FPR95 and by **3.31%** in the average AUROC, and our RankWeight outperforms other approaches by **25.14%** in FPR95 and by **6.80%** in AUROC. Moreover, the joint use of RankFeat and RankWeight achieves the best performance, reducing FPR95 by **44.72%** and improving AUROC by **8.19%** compared with previous approaches.

5.3 Ablation Studies

In this subsection, we conduct ablation studies based on ResNetv2-101. Unless explicitly specified, our RankFeat is applied to the Block 4 feature by default.

5.3.1 Removing the Rank-1 Matrix Outperforms Keeping it

Instead of removing the rank-1 matrix, another seemingly promising approach is keeping only the rank-1 matrix and abandoning the rest of the matrix. Table 7 presents the evaluation results of keeping only the rank-1 matrix. The performance falls behind that of removing the rank-1 feature by 18.8% in FPR95, which indicates that keeping only the rank-1 feature is inferior to removing it in distinguishing the two distributions. Nonetheless, it is worth noting that even keeping only the rank-1 matrix achieves very competitive performance against previous best methods, such as GradNorm [3] and ReAct [6].

5.3.2 Removing the Rank-1 Matrix Outperforms Removing the Rank- n Matrix ($n > 1$)

We evaluate the impact of removing the matrix of a higher rank, i.e., performing $\mathbf{X} - \sum_{i=1}^n \mathbf{s}_i \mathbf{u}_i \mathbf{v}_i^T$ where $n > 1$ for the high-level feature \mathbf{X} . Table 7 compares the performance of removing the rank-2 matrix and rank-3 matrix. When the rank of the removed matrix is increased, the average performance degrades accordingly. This demonstrates that removing the rank-1 matrix is the most effective approach to separate ID and OOD data. This result is coherent with the finding in Fig. 1(a): only the largest singular value of OOD data is significantly different from that of ID data. Therefore, removing the rank-1 matrix achieves the best performance.

TABLE 9: The approximate solution by PI yields competitive performance and costs much less time consumption. The test batch size is set as 16.

Computation Technique	Processing Time Per Image (ms)	iNaturalist		SUN		Places		Textures		Average	
		FPR95 (↓)	AUROC (↑)	FPR95 (↓)	AUROC (↑)	FPR95 (↓)	AUROC (↑)	FPR95 (↓)	AUROC (↑)	FPR95 (↓)	AUROC (↑)
GradNorm [3]	80.01	50.03	90.33	46.48	89.03	60.86	84.82	61.42	81.07	54.70	86.71
ReAct [6]	8.79	44.52	91.81	52.71	90.16	62.66	87.83	70.73	76.85	57.66	86.67
SVD	18.01	46.54	81.49	27.88	92.18	38.26	88.34	46.06	89.33	39.69	87.84
PI (#100 iter)	9.97	46.59	81.49	27.93	92.18	38.28	88.34	46.09	89.33	39.72	87.84
PI (#50 iter)	9.47	46.58	81.49	27.93	92.17	38.24	88.34	46.12	89.32	39.72	87.83
PI (#20 iter)	9.22	46.58	81.48	27.93	92.15	38.28	88.31	46.10	89.33	39.75	87.82
PI (#10 iter)	9.03	46.77	81.29	28.21	91.84	38.44	87.94	46.08	89.37	39.88	87.61
PI (#5 iter)	9.00	48.34	79.81	30.44	89.71	41.33	84.97	45.34	89.41	41.36	85.98

5.3.3 Block 3 and Block 4 Features are the Most Informative

In addition to exploring the high-level features at Block 3 and Block 4, we also investigate the possibility of applying RankFeat to features at shallow network layers. As shown in Table 8, the performances of RankFeat at the Block 1 and Block 2 features are not comparable to those at deeper layers. This is mainly because the shallow low-level features do not embed as rich semantic information as the deep features. Consequently, removing the rank-1 matrix of shallow features would not help to separate ID/OOD data.

5.3.4 Approximate PI Yields Competitive Performance

Table 9 compares the time consumption and performance of SVD and PI, as well as two recent *state-of-the-art* OOD methods ReAct and GradNorm. The performance of PI starts to become competitive against that of SVD ($< 0.1\%$) from 20 iterations on with **48.41%** time reduction. Compared with ReAct, the PI-based RankFeat only requires marginally 4.89% more time consumption. GradNorm is not comparable against other baselines in terms of time cost because it does not support the batch mode.

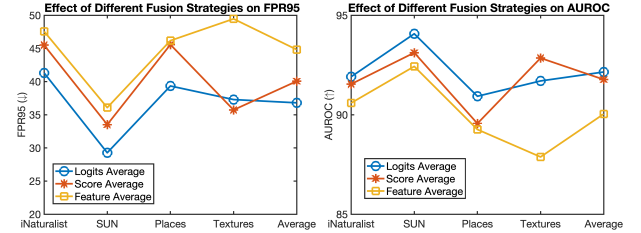


Fig. 9: The impact of fusion strategies on FPR95 and AUROC.

5.3.5 Logit Fusion Achieves the Best Performance

Fig. 9 displays the performance of different fusion strategies in combining RankFeat at the Block 3 and Block 4 features. As can be observed, averaging the logits outperforms other fusion strategies in most datasets and metrics. This indicates that fusing the logits can best coordinate and complement the benefit of both features at different depths.

TABLE 10: Impact of RankWeight when pruning different numbers of successive layers before the fully-connected layer.

# Layer	iNaturalist		SUN		Places		Textures		Average	
	FPR95 (↓)	AUROC (↑)	FPR95 (↓)	AUROC (↑)	FPR95 (↓)	AUROC (↑)	FPR95 (↓)	AUROC (↑)	FPR95 (↓)	AUROC (↑)
1	12.97	96.01	10.64	97.46	15.64	96.30	25.27	95.01	16.13	96.20
2	16.66	94.87	10.24	97.43	15.05	96.31	24.57	94.88	16.63	95.87
3	15.15	95.22	11.26	97.28	16.12	96.21	26.26	94.66	17.20	95.84

5.3.6 Pruning only One Layer is Sufficient

An interesting question about RankWeight is how many layers we need to prune. Table 10 compares the performance of RankWeight when pruning more layers. We can observe that adding more layers does not really help in improving the performance, and pruning a single layer is sufficient. The importance of this layer also implies that the over-confidence of OOD samples is more likely to happen in the last parametric layer before the fully-connected layer.

5.3.7 Pruning the Last Layer is Most Effective

TABLE 11: Impact of RankWeight when pruning weight matrices at different depths on ResNetv2-101.

Block	iNaturalist		SUN		Places		Textures		Average	
	FPR95 (↓)	AUROC (↑)	FPR95 (↓)	AUROC (↑)	FPR95 (↓)	AUROC (↑)	FPR95 (↓)	AUROC (↑)	FPR95 (↓)	AUROC (↑)
4	12.97	96.01	10.64	97.46	15.64	96.30	25.27	95.01	16.13	96.20
3	51.35	91.25	38.46	92.48	50.85	88.58	42.32	91.44	45.75	90.94
2	46.89	80.68	33.68	89.34	42.97	85.39	44.17	89.71	41.93	86.28
1	44.10	82.40	33.17	89.93	44.59	85.00	44.68	89.60	41.64	86.73

Table 11 presents the evaluation results of applying RankWeight at different depths. As can be seen, performing RankWeight at earlier layers will greatly deteriorate the performance. This indicates that applying our RankWeight to prune the last layer is most effective.

6 CONCLUSION

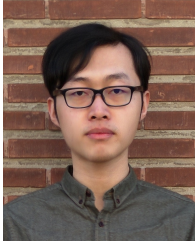
In this paper, we present RankFeat and RankWeight, two simple yet effective approaches for *post hoc* OOD detection. RankFeat performs OOD detection by removing the rank-1 matrix composed of the largest singular value from the high-level feature, while RankWeight similarly removes the rank-1 matrix from the parameter matrices of only one deep layer. We demonstrate its superior empirical results and the general applicability across architectures, network depths, different composability, and various benchmarks. Extensive ablation studies and comprehensive theoretical analyses are conducted to reveal important insights and to explain the working mechanism of our method.

REFERENCES

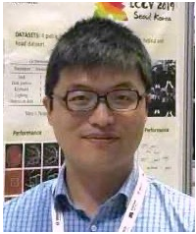
- [1] A. Nguyen, J. Yosinski, and J. Clune, "Deep neural networks are easily fooled: High confidence predictions for unrecognizable images," in *CVPR*, 2015, pp. 427–436.
- [2] H. Wang, W. Liu, A. Bocchieri, and Y. Li, "Can multi-label classification networks know what they don't know?" *NeurIPS*, vol. 34, 2021.
- [3] R. Huang, A. Geng, and Y. Li, "On the importance of gradients for detecting distributional shifts in the wild," *NeurIPS*, vol. 34, 2021.
- [4] K. Bibas, M. Feder, and T. Hassner, "Single layer predictive normalized maximum likelihood for out-of-distribution detection," *NeurIPS*, vol. 34, 2021.
- [5] J. Diffenderfer, B. Bartoldson, S. Chaganti, J. Zhang, and B. Kailkhura, "A winning hand: Compressing deep networks can improve out-of-distribution robustness," *NeurIPS*, vol. 34, 2021.
- [6] Y. Sun, C. Guo, and Y. Li, "React: Out-of-distribution detection with rectified activations," *NeurIPS*, vol. 34, 2021.
- [7] I. Gibbs and E. Candes, "Adaptive conformal inference under distribution shift," *NeurIPS*, vol. 34, 2021.
- [8] S. Fort, J. Ren, and B. Lakshminarayanan, "Exploring the limits of out-of-distribution detection," *NeurIPS*, vol. 34, 2021.
- [9] T. Sutter, A. Krause, and D. Kuhn, "Robust generalization despite distribution shift via minimum discriminating information," *NeurIPS*, vol. 34, 2021.
- [10] H. Ye, C. Xie, T. Cai, R. Li, Z. Li, and L. Wang, "Towards a theoretical framework of out-of-distribution generalization," *NeurIPS*, vol. 34, 2021.
- [11] A. Kumar, A. Raghunathan, R. Jones, T. Ma, and P. Liang, "Fine-tuning can distort pretrained features and underperform out-of-distribution," *ICLR*, 2022.
- [12] S. Garg, S. Balakrishnan, Z. C. Lipton, B. Neyshabur, and H. Sedghi, "Leveraging unlabeled data to predict out-of-distribution performance," *ICLR*, 2022.
- [13] A. Zaeemzadeh, N. Bisagno, Z. Sambugaro, N. Conci, N. Rahnavard, and M. Shah, "Out-of-distribution detection using union of 1-dimensional subspaces," in *CVPR*, 2021, pp. 9452–9461.
- [14] X. Du, Z. Wang, M. Cai, and Y. Li, "Vos: Learning what you don't know by virtual outlier synthesis," *ICLR*, 2022.
- [15] E. D. C. Gomes, F. Alberge, P. Duhamel, and P. Piantanida, "Igeood: An information geometry approach to out-of-distribution detection," *ICLR*, 2022.
- [16] M. Haroush, T. Frostig, R. Heller, and D. Soudry, "A statistical framework for efficient out of distribution detection in deep neural networks," in *ICLR*, 2022.
- [17] H. Wang, Z. Li, L. Feng, and W. Zhang, "Vim: Out-of-distribution with virtual-logit matching," in *CVPR*, 2022.
- [18] A. Djuricic, N. Bozanic, A. Ashok, and R. Liu, "Extremely simple activation shaping for out-of-distribution detection," *ICLR*, 2023.
- [19] Y. Sun and Y. Li, "Dice: Leveraging sparsification for out-of-distribution detection," in *ECCV*. Springer, 2022.
- [20] J. Zhang, J. Yang, P. Wang, H. Wang, Y. Lin, H. Zhang, Y. Sun, X. Du, K. Zhou, W. Zhang *et al.*, "Openood v1. 5: Enhanced benchmark for out-of-distribution detection," *arXiv preprint arXiv:2306.09301*, 2023.
- [21] J. Park, Y. G. Jung, and A. B. J. Teoh, "Nearest neighbor guidance for out-of-distribution detection," in *ICCV*, 2023.
- [22] J. Park, J. C. L. Chai, J. Yoon, and A. B. J. Teoh, "Understanding the feature norm for out-of-distribution detection," in *ICCV*, 2023.
- [23] X. Guan, Z. Liu, W.-S. Zheng, Y. Zhou, and R. Wang, "Revisit pca-based technique for out-of-distribution detection," in *ICCV*, 2023.
- [24] K. Lee, K. Lee, H. Lee, and J. Shin, "A simple unified framework for detecting out-of-distribution samples and adversarial attacks," *NeurIPS*, vol. 31, 2018.
- [25] K. He, X. Zhang, S. Ren, and J. Sun, "Deep residual learning for image recognition," in *CVPR*, 2016, pp. 770–778.
- [26] M. Xu, K. Wang, and Z. Lian, "Vra: Variational rectified activation for out-of-distribution detection," *NeurIPS*, 2023.
- [27] W. Liu, X. Wang, J. Owens, and Y. Li, "Energy-based out-of-distribution detection," *NeurIPS*, vol. 33, pp. 21 464–21 475, 2020.
- [28] Y. Song, N. Sebe, and W. Wang, "Rankfeat: Rank-1 feature removal for out-of-distribution detection," in *NeurIPS*, 2022.
- [29] D. J. Hand, "Classifier technology and the illusion of progress," *Statistical science*, vol. 21, no. 1, pp. 1–14, 2006.
- [30] J. Quiñero-Candela, M. Sugiyama, A. Schwaighofer, and N. D. Lawrence, *Dataset shift in machine learning*. MIT Press, 2008.
- [31] P. W. Koh, S. Sagawa, H. Marklund, S. M. Xie, M. Zhang, A. Balsubramani, W. Hu, M. Yasunaga, R. L. Phillips, I. Gao *et al.*, "Wilds: A benchmark of in-the-wild distribution shifts," in *ICML*. PMLR, 2021, pp. 5637–5664.
- [32] O. Wiles, S. Goyal, F. Stimberg, S. Alvisi-Rebuffi, I. Ktena, T. Cemgil *et al.*, "A fine-grained analysis on distribution shift," *ICLR*, 2022.
- [33] D. Hendrycks and T. Dietterich, "Benchmarking neural network robustness to common corruptions and perturbations," in *ICLR*, 2019.
- [34] Y. Ovadia, E. Fertig, J. Ren, Z. Nado, D. Sculley, S. Nowozin, J. Dillon, B. Lakshminarayanan, and J. Snoek, "Can you trust your model's uncertainty? evaluating predictive uncertainty under dataset shift," *NeurIPS*, vol. 32, 2019.
- [35] Y.-C. Hsu, Y. Shen, H. Jin, and Z. Kira, "Generalized odin: Detecting out-of-distribution image without learning from out-of-distribution data," in *CVPR*, 2020, pp. 10 951–10 960.
- [36] Y. Sun, X. Wang, Z. Liu, J. Miller, A. Efros, and M. Hardt, "Test-time training with self-supervision for generalization under distribution shifts," in *ICML*. PMLR, 2020, pp. 9229–9248.

- [37] D. Hendrycks, N. Mu, E. D. Cubuk, B. Zoph, J. Gilmer, and B. Lakshminarayanan, "Augmix: A simple data processing method to improve robustness and uncertainty," in *ICLR*, 2019.
- [38] S. Liang, Y. Li, and R. Srikant, "Enhancing the reliability of out-of-distribution image detection in neural networks," *ICLR*, 2018.
- [39] K. Han, A. Vedaldi, and A. Zisserman, "Learning to discover novel visual categories via deep transfer clustering," in *ICCV*, 2019, pp. 8401–8409.
- [40] Z. Zhong, E. Fini, S. Roy, Z. Luo, E. Ricci, and N. Sebe, "Neighborhood contrastive learning for novel class discovery," in *CVPR*, 2021, pp. 10867–10875.
- [41] W. J. Scheirer, A. de Rezende Rocha, A. Sapkota, and T. E. Boult, "Toward open set recognition," *IEEE TPAMI*, 2012.
- [42] S. Vaze, K. Han, A. Vedaldi, and A. Zisserman, "Open-set recognition: A good closed-set classifier is all you need," in *ICLR*, 2022.
- [43] D. Abati, A. Porrello, S. Calderara, and R. Cucchiara, "Latent space autoregression for novelty detection," in *CVPR*, 2019, pp. 481–490.
- [44] J. Tack, S. Mo, J. Jeong, and J. Shin, "Csi: Novelty detection via contrastive learning on distributionally shifted instances," *NeurIPS*, vol. 33, pp. 11839–11852, 2020.
- [45] C. Chow, "On optimum recognition error and reject tradeoff," *IEEE Transactions on information theory*, vol. 16, no. 1, pp. 41–46, 1970.
- [46] G. Fumera and F. Roli, "Support vector machines with embedded reject option," in *International Workshop on Support Vector Machines*. Springer, 2002, pp. 68–82.
- [47] K. Lee, H. Lee, K. Lee, and J. Shin, "Training confidence-calibrated classifiers for detecting out-of-distribution samples," *ICLR*, 2018.
- [48] A. Malinin and M. Gales, "Predictive uncertainty estimation via prior networks," *NeurIPS*, 2018.
- [49] Y. Geifman and R. El-Yaniv, "Selectivenet: A deep neural network with an integrated reject option," in *ICML*. PMLR, 2019.
- [50] M. Hein, M. Andriushchenko, and J. Bitterwolf, "Why relu networks yield high-confidence predictions far away from the training data and how to mitigate the problem," in *CVPR*, 2019.
- [51] A. Meinke and M. Hein, "Towards neural networks that provably know when they don't know," *ICLR*, 2020.
- [52] T. Jeong and H. Kim, "Ood-maml: Meta-learning for few-shot out-of-distribution detection and classification," *NeurIPS*, 2020.
- [53] J. Van Amersfoort, L. Smith, Y. W. Teh, and Y. Gal, "Uncertainty estimation using a single deep deterministic neural network," in *ICML*. PMLR, 2020.
- [54] J. Yang, H. Wang, L. Feng, X. Yan, H. Zheng, W. Zhang, and Z. Liu, "Semantically coherent out-of-distribution detection," in *ICCV*, 2021.
- [55] H. Wei, R. Xie, H. Cheng, L. Feng, B. An, and Y. Li, "Mitigating neural network overconfidence with logit normalization," in *ICML*. PMLR, 2022.
- [56] X. Du, X. Wang, G. Gozum, and Y. Li, "Unknown-aware object detection: Learning what you don't know from videos in the wild," in *CVPR*, 2022.
- [57] J. Katz-Samuels, J. B. Nakhleh, R. Nowak, and Y. Li, "Training ood detectors in their natural habitats," in *ICML*. PMLR, 2022.
- [58] J. Yang, K. Zhou, Y. Li, and Z. Liu, "Generalized out-of-distribution detection: A survey," *arXiv preprint arXiv:2110.11334*, 2021.
- [59] A. Bendale and T. E. Boult, "Towards open set deep networks," in *CVPR*, 2016, pp. 1563–1572.
- [60] R. Huang and Y. Li, "Mos: Towards scaling out-of-distribution detection for large semantic space," in *CVPR*, 2021, pp. 8710–8719.
- [61] X. Fang, N. Han, W. K. Wong, S. Teng, J. Wu, S. Xie, and X. Li, "Flexible affinity matrix learning for unsupervised and semisupervised classification," *IEEE TNNLS*, 2018.
- [62] X. Fang, N. Han, G. Zhou, S. Teng, Y. Xu, and S. Xie, "Dynamic double classifiers approximation for cross-domain recognition," *IEEE Transactions on Cybernetics*, 2020.
- [63] N. Han, J. Wu, X. Fang, S. Teng, G. Zhou, S. Xie, and X. Li, "Projective double reconstructions based dictionary learning algorithm for cross-domain recognition," *IEEE TIP*, 2020.
- [64] D. P. Kingma and M. Welling, "Auto-encoding variational bayes," *ICLR*, 2014.
- [65] E. G. Tabak and C. V. Turner, "A family of nonparametric density estimation algorithms," *Communications on Pure and Applied Mathematics*, vol. 66, no. 2, pp. 145–164, 2013.
- [66] D. J. Rezende, S. Mohamed, and D. Wierstra, "Stochastic backpropagation and approximate inference in deep generative models," in *ICML*. PMLR, 2014, pp. 1278–1286.
- [67] A. Van den Oord, N. Kalchbrenner, L. Espeholt, O. Vinyals, A. Graves *et al.*, "Conditional image generation with pixelcnn decoders," *NeurIPS*, vol. 29, 2016.
- [68] L. Dinh, J. Sohl-Dickstein, and S. Bengio, "Density estimation using real nvp," *ICLR*, 2017.
- [69] X. Huang, Y. Li, O. Poursaeed, J. Hopcroft, and S. Belongie, "Stacked generative adversarial networks," in *CVPR*, 2017, pp. 5077–5086.
- [70] D. Jiang, S. Sun, and Y. Yu, "Revisiting flow generative models for out-of-distribution detection," in *ICLR*, 2022.
- [71] J. Ren, P. J. Liu, E. Fertig, J. Snoek, R. Poplin, M. Depristo, J. Dillon, and B. Lakshminarayanan, "Likelihood ratios for out-of-distribution detection," *NeurIPS*, vol. 32, 2019.
- [72] J. Serrà, D. Álvarez, V. Gómez, O. Slizovskaia, J. F. Núñez, and J. Luque, "Input complexity and out-of-distribution detection with likelihood-based generative models," in *ICLR*, 2019.
- [73] Z. Wang, B. Dai, D. Wipf, and J. Zhu, "Further analysis of outlier detection with deep generative models," *NeurIPS*, vol. 33, pp. 8982–8992, 2020.
- [74] Z. Xiao, Q. Yan, and Y. Amit, "Likelihood regret: An out-of-distribution detection score for variational auto-encoder," *NeurIPS*, vol. 33, pp. 20685–20696, 2020.
- [75] P. Kirichenko, P. Izmailov, and A. G. Wilson, "Why normalizing flows fail to detect out-of-distribution data," *NeurIPS*, vol. 33, pp. 20578–20589, 2020.
- [76] R. Schirmer, Y. Zhou, T. Ball, and D. Zhang, "Understanding anomaly detection with deep invertible networks through hierarchies of distributions and features," *NeurIPS*, vol. 33, pp. 21038–21049, 2020.
- [77] K. Kim, J. Shin, and H. Kim, "Locally most powerful bayesian test for out-of-distribution detection using deep generative models," *NeurIPS*, vol. 34, 2021.
- [78] L. Tao, X. Du, X. Zhu, and Y. Li, "Non-parametric outlier synthesis," *ICLR*, 2023.
- [79] X. Du, Y. Sun, X. Zhu, and Y. Li, "Dream the impossible: Outlier imagination with diffusion models," *NeurIPS*, 2023.
- [80] E. Nalisnick, A. Matsukawa, Y. W. Teh, D. Gorur, and B. Lakshminarayanan, "Do deep generative models know what they don't know?" in *ICLR*, 2019.
- [81] K. He, X. Zhang, S. Ren, and J. Sun, "Identity mappings in deep residual networks," in *ECCV*. Springer, 2016, pp. 630–645.
- [82] V. A. Marčenko and L. A. Pastur, "Distribution of eigenvalues for some sets of random matrices," *Mathematics of the USSR-Sbornik*, vol. 1, no. 4, p. 457, 1967.
- [83] A. M. Sengupta and P. P. Mitra, "Distributions of singular values for some random matrices," *Physical Review E*, vol. 60, no. 3, p. 3389, 1999.
- [84] J. Deng, W. Dong, R. Socher, L.-J. Li, K. Li, and L. Fei-Fei, "Imagenet: A large-scale hierarchical image database," in *CVPR*. Ieee, 2009, pp. 248–255.
- [85] D. Hendrycks and K. Gimpel, "A baseline for detecting misclassified and out-of-distribution examples in neural networks," *ICLR*, 2017.
- [86] F. N. Iandola, S. Han, M. W. Moskewicz, K. Ashraf, W. J. Dally, and K. Keutzer, "Squeezenet: Alexnet-level accuracy with 50x fewer parameters and 0.5 mb model size," *ICLR*, 2017.
- [87] L. Yuan, Y. Chen, T. Wang, W. Yu, Y. Shi, Z.-H. Jiang, F. E. Tay, J. Feng, and S. Yan, "Tokens-to-token vit: Training vision transformers from scratch on imagenet," in *ICCV*, 2021.
- [88] A. Dosovitskiy, L. Beyer, A. Kolesnikov, D. Weissenborn, X. Zhai, T. Unterthiner, M. Dehghani, M. Minderer, G. Heigold, S. Gelly, J. Uszkoreit, and N. Houlsby, "An image is worth 16x16 words: Transformers for image recognition at scale," *ICLR*, 2021.
- [89] Z. Liu, Y. Lin, Y. Cao, H. Hu, Y. Wei, Z. Zhang, S. Lin, and B. Guo, "Swin transformer: Hierarchical vision transformer using shifted windows," in *ICCV*, 2021.
- [90] A. Krizhevsky, G. Hinton *et al.*, "Learning multiple layers of features from tiny images," 2009.
- [91] G. Van Horn, O. Mac Aodha, Y. Song, Y. Cui, C. Sun, A. Shepard, H. Adam, P. Perona, and S. Belongie, "The inaturalist species classification and detection dataset," in *CVPR*, 2018.
- [92] J. Xiao, J. Hays, K. A. Ehinger, A. Oliva, and A. Torralba, "Sun database: Large-scale scene recognition from abbey to zoo," in *CVPR*, 2010.

- [93] B. Zhou, A. Lapedriza, A. Khosla, A. Oliva, and A. Torralba, "Places: A 10 million image database for scene recognition," *IEEE TPAMI*, 2017.
- [94] M. Cimpoi, S. Maji, I. Kokkinos, S. Mohamed, and A. Vedaldi, "Describing textures in the wild," in *CVPR*, 2014.
- [95] D. Hendrycks, S. Basart, M. Mazeika, M. Mostajabi, J. Steinhardt, and D. Song, "Scaling out-of-distribution detection for real-world settings," *ICML*, 2022.
- [96] A. Kolesnikov, L. Beyer, X. Zhai, J. Puigcerver, J. Yung, S. Gelly, and N. Houlsby, "Big transfer (bit): General visual representation learning," in *ECCV*, 2020.
- [97] A. Dosovitskiy, L. Beyer, A. Kolesnikov, D. Weissenborn, X. Zhai, T. Unterthiner, M. Dehghani, M. Minderer, G. Heigold, S. Gelly *et al.*, "An image is worth 16x16 words: Transformers for image recognition at scale," in *ICLR*, 2021.
- [98] X. Ding, X. Zhang, N. Ma, J. Han, G. Ding, and J. Sun, "Repvgg: Making vgg-style convnets great again," in *CVPR*, 2021, pp. 13733–13742.
- [99] A. F. Emmott, S. Das, T. Dietterich, A. Fern, and W.-K. Wong, "Systematic construction of anomaly detection benchmarks from real data," in *Proceedings of the ACM SIGKDD workshop on outlier detection and description*, 2013.
- [100] I. Golan and R. El-Yaniv, "Deep anomaly detection using geometric transformations," *NeurIPS*, 2018.
- [101] I. J. Goodfellow, J. Shlens, and C. Szegedy, "Explaining and harnessing adversarial examples," *ICLR*, 2015.
- [102] M. Huh, H. Mobahi, R. Zhang, B. Cheung, P. Agrawal, and P. Isola, "The low-rank simplicity bias in deep networks," *TMLR*, 2023.
- [103] M. Andriushchenko, D. Bahri, H. Mobahi, and N. Flammarion, "Sharpness-aware minimization leads to low-rank features," *NeurIPS*, 2023.
- [104] P. Foret, A. Kleiner, H. Mobahi, and B. Neyshabur, "Sharpness-aware minimization for efficiently improving generalization," in *ICLR*, 2021.



Yue Song received the B.Sc. *cum laude* from KU Leuven, Belgium and the joint M.Sc. *summa cum laude* from the University of Trento, Italy and KTH Royal Institute of Technology, Sweden. Currently, he is a Ph.D. student with the Multimedia and Human Understanding Group (MHUG) at the University of Trento, Italy. His research interests are computer vision, deep learning, and numerical analysis and optimization.



Wei Wang is an Assistant Professor of Computer Science at University of Trento, Italy. Previously, after obtaining his PhD from University of Trento in 2018, he became a Postdoc at EPFL, Switzerland. His research interests include machine learning and its application to computer vision and multimedia analysis.



Nicu Sebe is Professor with the University of Trento, Italy, leading the research in the areas of multimedia information retrieval and human behavior understanding. He was the General Co-Chair of ACM Multimedia 2013, and the Program Chair of ACM Multimedia 2007 and 2011, ECCV 2016, ICCV 2017 and ICPR 2020. He is a fellow of the International Association for Pattern Recognition.

APPENDIX A MORE EVALUATION RESULTS

A.1 CIFAR100 with Different Architectures

TABLE 12: The evaluation results with different model architectures on CIFAR100 [90]. All values are reported in percentages, and these *post hoc* methods are directly applied to the model. The best three results are highlighted with **red**, **blue**, and **cyan**.

Model	Methods	iNaturalist		SUN		Places		Textures		Average	
		FPR95 (↓)	AUROC (↑)	FPR95 (↓)	AUROC (↑)	FPR95 (↓)	AUROC (↑)	FPR95 (↓)	AUROC (↑)	FPR95 (↓)	AUROC (↑)
RepVGG-A0 [98]	MSP [85]	61.55	85.03	91.05	69.19	65.45	82.10	86.68	65.56	76.18	75.47
	ODIN [38]	50.20	87.88	88.00	66.56	61.85	79.34	84.87	63.89	71.23	74.42
	Energy [27]	53.71	84.59	86.71	66.58	59.71	78.64	84.57	63.88	71.18	73.42
	Mahalanobis [24]	81.43	74.81	89.77	67.12	79.49	73.06	64.95	82.19	78.91	74.30
	GradNorm [3]	78.87	68.21	95.10	44.73	66.25	75.41	92.98	43.83	83.30	58.05
	ReAct [6]	48.09	93.00	73.87	78.12	61.63	78.43	75.23	81.36	64.71	82.73
	RankFeat	40.19	88.06	70.47	76.35	57.75	83.58	52.89	83.28	55.33	82.82
	RankWeight	46.16	89.90	75.18	77.63	77.80	75.24	53.58	85.57	63.18	82.09
	RankFeat + RankWeight	19.87	93.37	56.98	81.45	41.96	88.91	35.17	91.68	38.50	89.35
	MSP [85]	77.69	78.25	93.54	66.93	81.57	76.71	88.47	65.79	85.32	71.92
ResNet-56 [25]	ODIN [38]	66.92	79.25	95.05	50.45	77.45	72.88	90.51	53.47	82.48	64.01
	Energy [27]	65.24	79.13	95.05	49.33	77.10	72.32	90.39	52.68	81.95	63.37
	Mahalanobis [24]	89.47	69.32	91.38	54.76	82.32	77.53	68.83	79.64	83.00	70.31
	GradNorm [3]	96.72	42.09	94.19	47.97	94.61	48.09	89.14	50.18	93.67	47.08
	ReAct [6]	50.59	90.56	69.23	85.79	55.38	87.98	82.60	75.51	64.50	84.96
	RankFeat	34.62	88.21	61.82	80.50	53.79	89.71	30.89	91.31	45.28	87.43
	RankWeight	31.93	88.12	60.58	80.98	67.26	76.96	28.51	90.95	47.07	84.34
	RankFeat + RankWeight	15.67	93.12	53.78	88.91	39.95	90.85	22.74	92.71	33.04	91.40
	MSP [85]	77.69	78.25	93.54	66.93	81.57	76.71	88.47	65.79	85.32	71.92
	ODIN [38]	66.92	79.25	95.05	50.45	77.45	72.88	90.51	53.47	82.48	64.01

We also evaluate our method on the CIFAR benchmark with various model architectures. The evaluation OOD datasets are the same as those of the ImageNet-1k benchmark. We take ResNet-56 [25] and RepVGG-A0 [98] pre-trained on ImageNet-1k as the backbones, and then fine-tune them on CIFAR100 [90] for 100 epochs. The learning rate is initialized with 0.1 and is decayed by 10 every 30 epoch. Notice that this training process is to obtain a well-trained classifier but the ODO methods (including ours) are still *post hoc* and do not need any extra training.

Table 12 compares the performance against the *post hoc* baselines. Our RankFeat + RankWeight establishes the *state-of-the-art* performances across architectures on most datasets and metrics, outperforming the second best method by **26.21** % in the average FPR95 on RepVGG-A0 and by **31.46** % in the average FPR95 on ResNet-56. Applying RankFeat and RankWeight separately also achieves impressive results. Since the CIFAR images are small in resolution (*i.e.*, 32×32), the downsampling times and the number of feature blocks of the original models are reduced. We thus only apply RankFeat to the final feature before the GAP layer.

A.2 One-class CIFAR10

To further demonstrate the applicability of our method, we follow [44], [99], [100] and conduct experiments on one-class CIFAR10. The setup is as follows: we choose one of the classes as the ID set while keeping other classes as OOD sets. Table 13 reports the average AUROC on CIFAR10. Our RankFeat and RankWeight outperform other baselines on most subsets as well as on the average result.

TABLE 13: The average AUROC (%) on one-class CIFAR10 based on ResNet-56.

Methods	Plane	Car	Bird	Cat	Deer	Dog	Frog	Horse	Ship	Truck	Mean
MSP	59.75	52.48	62.96	48.73	59.15	52.39	67.33	59.34	54.55	51.97	56.87
Energy	83.12	91.56	68.99	56.02	75.03	77.33	69.50	88.41	82.88	84.74	77.76
ReAct	82.24	96.69	78.32	76.84	76.11	86.80	86.15	90.95	89.91	94.17	85.82
RankFeat	79.26	98.54	82.04	80.28	82.89	90.28	89.06	95.30	94.11	94.02	88.58
RankWeight	81.32	97.65	84.17	79.68	80.54	89.18	90.34	95.76	93.78	94.54	88.70
RankFeat+RankWeight	84.56	98.15	85.73	81.43	84.32	91.78	90.73	96.21	95.07	94.78	90.28

APPENDIX B

BASELINE METHODS

For the convenience of audiences, we briefly recap the previous *post hoc* methods for OOD detection. Some implementation details of the methods are also discussed.

MSP [85]. One of the earliest work considered directly using the Maximum Softmax Probability (MSP) as the scoring function for OOD detection. Let $f(\cdot)$ and \mathbf{x} denote the model and input, respectively. The MSP score can be computed as:

$$\text{MSP}(\mathbf{x}) = \max(\text{Softmax}(f(\mathbf{x}))) \quad (30)$$

Despite the simplicity of this approach, the MSP score often fails as neural networks could assign arbitrarily high confidences to the OOD data [1].

ODIN [38]. Based on MSP [85], ODIN [38] further integrated temperature scaling and input perturbation to better separate the ID and OOD data. The ODIN score is calculated as:

$$\text{ODIN}(\mathbf{x}) = \max\left(\text{Softmax}\left(\frac{f(\bar{\mathbf{x}})}{T}\right)\right) \quad (31)$$

where T is the hyper-parameter temperature, and $\bar{\mathbf{x}}$ denote the perturbed input. Following the setting in [3], we set $T=1000$. According to [3], the input perturbation does not bring any performance improvement on the ImageNet-1k benchmark. Hence, we do not perturb the input either.

Energy score [27]. Liu *et al.* [27] argued that an energy score is superior than the MSP because it is theoretically aligned with the input probability density, *i.e.*, the sample with a higher energy correspond to data with a lower likelihood of occurrence. Formally, the energy score maps the logit output to a scalar function as:

$$\text{Energy}(\mathbf{x}) = \log \sum_{i=1}^C \exp(f_i(\mathbf{x})) \quad (32)$$

where C denotes the number of classes.

Mahalanobis distance [24]. Lee *et al.* [24] proposed to model the Softmax outputs as the mixture of multivariate Gaussian distributions and use the Mahalanobis distance as the scoring function for OOD uncertainty estimation. The score is computed as:

$$\text{Mahalanobis}(\mathbf{x}) = \max_i \left(- (f(\mathbf{x}) - \mu_i)^T \Sigma (f(\mathbf{x}) - \mu_i) \right) \quad (33)$$

where μ_i denotes the feature vector mean, and Σ represents the covariance matrix across classes. Following [3], we use 500 samples randomly selected from ID datasets and an auxiliary tuning dataset to train the logistic regression and tune the perturbation strength ϵ . For the tuning dataset, we use FGSM [101] with a perturbation size of 0.05 to generate adversarial examples. The selected ϵ is set as 0.001 for ImageNet-1k.

GradNorm [3]. Huang *et al.* [3] proposed to estimate the OOD uncertainty by utilizing information extracted from the gradient space. They compute the KL divergence between the Softmax output and a uniform distribution, and back-propagate the gradient to the last layer. Then the vector norm of the gradient is used as the scoring function. Let \mathbf{w} and \mathbf{u} denote the weights of last layer and the uniform distribution. The score is calculated as:

$$\text{GradNorm}(\mathbf{x}) = \left\| \frac{\partial D_{KL}(\mathbf{u} \parallel \text{Softmax}(f(\mathbf{x})))}{\partial \mathbf{w}} \right\|_1 \quad (34)$$

where $\|\cdot\|_1$ denotes the L_1 norm, and $D_{KL}(\cdot)$ represents the KL divergence measure.

ReAct [6]. In [6], the authors observed that the activations of the penultimate layer are quite different for ID and OOD data. The OOD data is biased towards triggering very high activations, while the ID data has the well-behaved mean and deviation. In light of this finding, they propose to clip the activations as:

$$f_{l-1}(\mathbf{x}) = \min(f_{l-1}(\mathbf{x}), \tau) \quad (35)$$

where $f_{l-1}(\cdot)$ denotes the activations for the penultimate layer, and τ is the upper limit computed as the 90-th percentile of activations of the ID data. Finally, the Energy score [27] is computed for estimating the OOD uncertainty.

ASH [18]. Following ReAct [6], ASH considers more diverse activation-shaping approaches beyond clipping. They consider three variants to perturb the activations:

- **ASH-P:** the activations are pruned according to the threshold calculated as the p -th percentile of activations;
- **ASH-B:** after clipping and zeroing out the activations, all non-zero values are scaled by the sparsity of activations;
- **ASH-S:** after clipping and zeroing out the activations, all non-zero values are scaled by a hyper-parameter calculated as the ratio between the sum of non-zero activations and the sparsity of the activations;

We observe that on the ImageNet-1k benchmark, ASH-S achieves the best performance. We also use ASH-S and compute hyper-parameters from the statistics of the ID set.

VRA [26]. Motivated by ReAct [6], VRA leverages the variational formulation to seek the optimal activation function by extra suppression and amplification. The modified activation function takes the form:

$$\text{VRA}(z) = \begin{cases} 0, & z < \alpha \\ z + \gamma, & \alpha < z < \beta \\ \beta, & z > \beta \end{cases} \quad (36)$$

where z denotes the original activation, α , β , and γ are the hyper-parameters that control the thresholds and the extents of suppression/amplification. We compute these hyper-parameters based on the variational objective of VRA.

Interestingly, motivated by our RankFeat, VRA also conducts some similar upper bound analyses. They show that their upper bound can be formulated as:

$$\text{VRA}(z) \leq k_2 \|\mathbf{W}\|_p \|\mathbf{z}\|_p + k_2 \|\mathbf{b}\|_p + \log(Q) \quad (37)$$

where k_2 is a constant upper-bounding the relation $\|f(z)\|_\infty < k_2 \|f(z)\|_p$. According to the above inequality, maximizing $\mathbb{E}_{in}[z] - \mathbb{E}_{out}[z]$ is also equivalent to maximizing the upper bound gap between ID and OOD data.

APPENDIX C

VISUALIZATION ABOUT RANKFEAT

C.1 Singular Value Distributions

Fig. 10 compares the top-5 singular value distribution of ID and OOD feature matrices on all the datasets. Our novel observation consistently holds for every OOD dataset: the dominant singular value s_1 of OOD feature always tends to be significantly larger than that of ID feature.

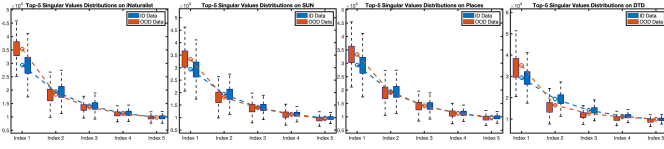


Fig. 10: The top-5 singular value distribution of the ID dataset and OOD datasets. The first singular values s_1 of OOD data are consistently much larger than those of ID data on each OOD dataset.

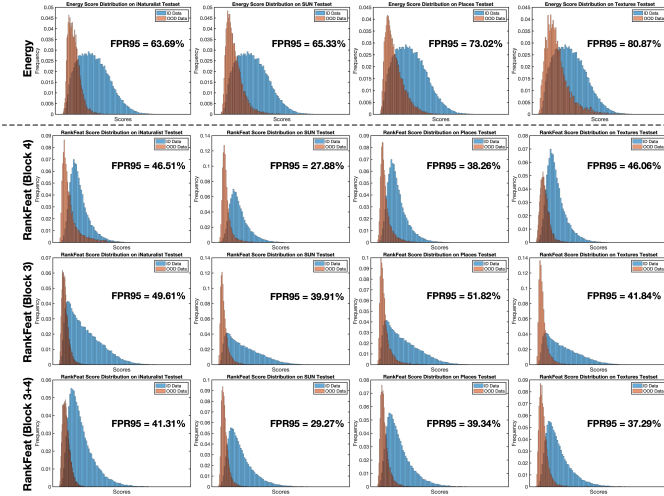


Fig. 11: The score distributions of *Energy* [27] (top row) and our proposed *RankFeat* (rest rows) on four OOD datasets. Our *RankFeat* applies to different high-level features at the later depths of the network, and their score functions can be further fused.

C.2 Score Distributions

Fig. 11 displays the score distributions of *RankFeat* at Block 3 and Block 4, as well as the fused results. Our *RankFeat* works for both high-level features. For the score fusion, when Block 3 and Block 4 features are of similar scores ($diff. < 5\%$), the feature combination could have further improvements.

C.3 Output Distributions

Fig. 12(a) presents the output distribution (*i.e.*, the logits after Softmax layer) on ImageNet and iNaturalist. After our *RankFeat*, the OOD data have a larger reduction in the probability output; most of OOD predictions are of very small probabilities (< 0.1).

C.4 Logit Distributions

Fig. 12(b) displays the logits distribution of our *RankFeat*. The OOD logits after *RankFeat* have much less variations and therefore are closer to the uniform distribution.

APPENDIX D

WHY ARE THE SINGULAR VALUE DISTRIBUTIONS OF ID AND OOD FEATURES DIFFERENT?

In the paper, we give some theoretical analysis to explain the working mechanism of our *RankFeat*. It would be also interesting to investigate why the singular value distributions

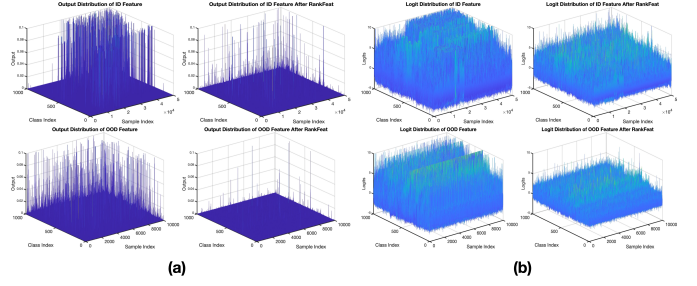


Fig. 12: (a) Output distributions of *RankFeat*. (b) Logit distributions of *RankFeat*.

of the ID and OOD features are different. Here we give an intuitive conjecture. Since the network is well trained on the ID training set, when encountered with ID data, the feature matrix is likely to be more informative. Accordingly, more singular vectors would be active and the matrix energies spread over the corresponding singular values, leading to a more flat spectrum. On the contrary, for the unseen OOD data, the feature is prone to have a more compact representation, and less singular vectors might be active. In this case, the dominant singular value of OOD feature would be larger and would take more energies of the matrix. The informativeness can also be understood by considering applying PCA on the feature matrix. Suppose that we are using PCA to reduce the dimension of ID and OOD feature to 1. The amount of retained information can be measured by explained variance (%). The metric is defined as $\sum_{i=0}^k s_i^2 / \sum_{j=0}^n s_j^2$ where k denotes the projected dimension and n denotes the total dimension. It measures the portion of variance that the projected data could account for. We compute the average explained variance of all datasets and present the result in Table 14.

TABLE 14: The average explained variance ratio (%) of the ID and OOD datasets.

Dataset	ImageNet-1k	iNaturalist	SUN	Places	Textures
Explained Variance (%)	28.57	38.74	35.79	35.17	42.21

As can be observed, the OOD datasets have a larger explained variance ratio than the ID dataset. *That being said, to retain the same amount of information, we need fewer dimensions for the projection of OOD features. This indicates that the information of OOD feature is easier to be captured and the OOD feature matrix is thus less informative.*

As for how the training leads to the difference, we doubt that the well-trained network weights might cause and amplify the gap in the dominant singular value of the ID and OOD feature. To verify this guess, we compute the singular values distributions of the Google BiT-S ResNet2-100 model [81], [96] with different training steps, as well as a randomly initialized network as the baseline.

Fig. 13 depicts the top-5 largest singular value distributions of the network with different training steps. Unlike the trained networks, the untrained network with random weights has quite a similar singular value distribution for the ID and OOD data. The singular values of both ID and OOD features are of similar magnitudes with the untrained network. However, when the number of training

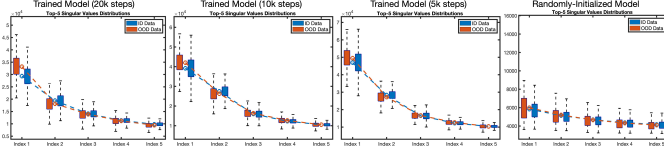


Fig. 13: The top-5 largest singular value distributions of the pre-trained network with different training steps. For the untrained network initialized with random weights, the singular values distributions of ID and OOD features exhibit very similar behaviors. As the training step increases, the difference between the largest singular value is gradually amplified.

steps is increased, the gap of dominant singular value between ID and OOD feature is magnified accordingly. This phenomenon supports our conjecture that the well-trained network weights cause and amplify the difference of the largest singular value. Interestingly, our finding is coherent with [42]. In [42], the authors demonstrate that the classification accuracy of a model is highly correlated with its ability of OOD detection and open-set recognition. Training a stronger model could naturally improve the OOD detection performance. We empirically show that the gap of the dominant singular value is gradually amplifying as the training goes on, which serves as supporting evidence for [42].

On the theoretical side, Huh *et al.* [102] reveal that in general over-parameterized neural networks are biased towards finding low-rank embeddings for input data. Further, Andriushchenko *et al.* [103] present theoretical guarantees that using Sharpness-Aware Minimization (SAM) [104] provably leads to low-rank features for a diverse set of architectures. Although the conjecture has only been proved for SAM, it is known that many of its properties are generalized to other commonly used optimizers. These works provide some other theoretical evidence to support our argument.

APPENDIX E

THEOREM AND PROOF OF MANCHENKO-PASTUR LAW

In the paper, we use the MP distribution of random matrices to show that removing the rank-1 matrix makes the statistics of OOD features closer to random matrices. For self-containment and readers' convenience, here we give a brief proof of Manchenko-Pastur Law.

Theorem 2. Let \mathbf{X} be a random matrix of shape $t \times n$ whose entries are random variables with $E(\mathbf{X}_{ij}) = 0$ and $E(\mathbf{X}_{ij}^2) = 1$. Then the eigenvalues of the sample covariance $\mathbf{Y} = \frac{1}{n}\mathbf{X}\mathbf{X}^T$ converges to the probability density function: $\rho(\lambda) = \frac{t}{n} \frac{\sqrt{(\lambda_+ - \lambda)(\lambda - \lambda_-)}}{2\pi\lambda\sigma^2}$ for $\lambda \in [\lambda_-, \lambda_+]$ where $\lambda_- = \sigma^2(1 - \sqrt{\frac{n}{t}})^2$ and $\lambda_+ = \sigma^2(1 + \sqrt{\frac{n}{t}})^2$.

Proof. Similar with the deduction of our bound analysis, the sample covariance \mathbf{Y} can be written as the sum of rank-1 matrices:

$$\mathbf{Y} = \sum_{s=0}^t \mathbf{Y}_n^s, \quad \mathbf{Y}_n^s = \mathbf{U}_n^s \mathbf{D}_n^s (\mathbf{U}_n^s)^* \quad (38)$$

where \mathbf{U}_n^s is a unitary matrix, and \mathbf{D}_n^s is a diagonal matrix with the only eigenvalue $\beta = n/t$ for large n (rank-1 matrix). Then we can compute the Stieltjes transform of each \mathbf{Y}_n^s as:

$$s_n(z) = \frac{1}{n} \text{tr}(\mathbf{Y}_n^s - z\mathbf{I})^{-1} \quad (39)$$

Relying on Neumann series, the above equation can be re-written as:

$$\begin{aligned} s_n(z) &= -\frac{1}{n} \sum_{k=0}^{\infty} \frac{\text{tr}(\mathbf{Y}_n^s)^k}{z^{k+1}} \\ &= -\frac{1}{n} \left(\frac{n}{z} + \sum_{k=1}^{\infty} \frac{\beta^k}{z^{k+1}} \right) \\ &= -\frac{1}{n} \left(\frac{n-1}{z} + \frac{1}{z-\beta} \right) \end{aligned} \quad (40)$$

Let $z := z_n(s)$ and we can find the function inverse of the transform:

$$nsz_n(s)^2 - n(s\beta - 1)z_n(s) - (n-1)\beta = 0 \quad (41)$$

The close-formed solution is calculated as:

$$\begin{aligned} z_n(s) &= \frac{n(s\beta - 1) \pm \sqrt{n^2(s\beta - 1)^2 + 4n(n-1)s\beta}}{2ns} \\ &\approx \frac{1}{2ns} \left(n(s\beta - 1) \pm \left| n(s\beta + 1) - \frac{2s\beta}{\beta + 1} \right| \right) \end{aligned} \quad (42)$$

For large n , the term $\frac{2s\beta}{\beta + 1}$ is sufficiently small and we can omit it. The solution is defined as:

$$z_n(s) = -\frac{1}{s} + \frac{\beta}{n(1 + s\beta)} \quad (43)$$

The R transform of each \mathbf{Y}_n^s is given by:

$$R_{\mathbf{Y}_n^s}(s) = z_n(-s) - \frac{1}{s} = \frac{\beta}{n(1 - s\beta)} \quad (44)$$

Accordingly, the R transform for \mathbf{Y}_n is given by:

$$R_{\mathbf{Y}}(s) = tR_{\mathbf{Y}_n^s}(s) = \frac{\beta t}{n(1 - s\beta)} = \frac{1}{1 - s\beta} \quad (45)$$

Thus, the inverse Stieltjes transform of \mathbf{Y} is

$$z(s) = -\frac{1}{s} + \frac{1}{1 + s\beta} \quad (46)$$

Then the Stieltjes transform of \mathbf{Y} is computed by inverting the above equation as:

$$s(z) = \frac{-(z + \beta + 1) + \sqrt{(z + \beta + 1)^2 - 4\beta z}}{2z\beta} \quad (47)$$

Since $\beta = n/t$, finding the limiting distribution of the above equation directly gives the Manchenko-Pastur distribution:

$$\begin{aligned} \rho(\lambda) &= \frac{t}{n} \frac{\sqrt{(\lambda_+ - \lambda)(\lambda - \lambda_-)}}{2\pi\lambda\sigma^2} \text{ for } \lambda \in [\lambda_-, \lambda_+], \\ \lambda_- &= \sigma^2(1 - \sqrt{\frac{n}{t}})^2, \lambda_+ = \sigma^2(1 + \sqrt{\frac{n}{t}})^2 \end{aligned} \quad (48)$$

The theorem is thus proved. \square